

ALMA MATER STUDIORUM – UNIVERSITÀ DI BOLOGNA
SEDE DI CESENA
SECONDA FACOLTÀ DI INGEGNERIA CON SEDE A CESENA
CORSO DI LAUREA SPECIALISTICA IN INGEGNERIA BIOMEDICA

**THE EFFECTS OF HYPOCALCEMIA ON
SPATIAL ALTERNANS AND
VENTRICULAR FIBRILLATION
STUDIED WITH THE OPTICAL
MAPPING TECHNIQUE**

Tesi in

BIONGEGNERIA MOLECOLARE E CELLULARE

Relatore

Prof. Stefano Severi

Correlatore

Prof. Flavio H. Fenton

Presentata da

Marco Piangerelli

SESSIONE III

ANNO ACCADEMICO 2011-2012

To My Parents.

Contents

INTRODUCTION AND AIM.....	1
BIBLIOGRAPHY	3
1. THE HEART: ANATOMY AND PHYSIOLOGY	4
1.1 THE HEART.....	4
1.1.1 <i>Electrical activity and propagation</i>	<i>8</i>
1.2 EXCITATION-CONTRACTION COUPLING	10
1.2.1 <i>Action potentials: phases</i>	<i>10</i>
1.2.2 <i>Subcellular mechanisms: calcium cycle.....</i>	<i>12</i>
1.3 CARDIAC CYCLE.....	12
1.4 CARDIAC ARRHYTHMIAS.....	15
1.4.1 <i>Arrhythmias: definition and classification.....</i>	<i>15</i>
1.4.2 <i>Anatomical and functional reentry</i>	<i>16</i>
1.5 CLINICAL TREATMENTS FOR ARRHYTHMIAS	17
BIBLIOGRAPHY	19
2. ALTERNANS AND THEIR ROLE IN CARDIAC ARRHYTHMIAS	22
2.1 ALTERNANS: DEFINITION AND FIRST CONCEPTS	22
2.2 THE RESTITUTION RELATION.....	23
2.2.1 <i>The mechanism of APD alternans</i>	<i>25</i>
2.2.2 <i>Bifurcations</i>	<i>26</i>
2.3 A MORE COMPLICATED APD RESTITUTION RELATION: THE MEMORY EFFECT.....	29
2.3.1 <i>Experiments vs theory.....</i>	<i>29</i>
2.3.2 <i>A new stability criterion</i>	<i>30</i>
2.4 ALTERNANS IN CARDIAC TISSUE	32
2.4.1 <i>Concordant and discordant alternans.....</i>	<i>32</i>
2.4.2 <i>Electrical propagating waves.....</i>	<i>33</i>
2.5 ...TO SUM UP.....	33
BIBLIOGRAPHY	35

3. THE EXPERIMENTAL PROTOCOL	38
3.1 DATA ACQUISITION: THE OPTICAL MAPPING TECHNIQUE	38
3.1.1 <i>Voltage-sensitive dyes and detectors</i>	38
3.2 DATA COLLECTING: THE PREPARATION OF CARDIAC TISSUE	41
3.2.1 <i>The optical setup</i>	42
3.2.2 <i>Stimulation protocols</i>	45
3.3 DATA ANALYSIS: THE JAVA CODE	46
3.3.1 <i>Methods of analysis: filtering and removing signal drift.</i>	47
3.3.2 <i>Alternans phase definition</i>	49
3.3.3 <i>Restitution curves</i>	50
BIBLIOGRAPHY	51
4. RESULTS AND DISCUSSION	52
4.1 RESULTS	52
4.1.1 <i>The effects of hypocalcemia on VF</i>	52
4.1.2 <i>The effects of hypocalcemia on the slope of the dynamic restitution curves and on alternans</i>	53
4.1.3 <i>The effects of hypocalcemia On short-term memory</i>	59
4.1.4 <i>The Tolkacheva's criterion</i>	60
4.2 <i>Conclusions</i>	62
4.3 LIMITATIONS AND FUTURE WORKS	64
BIBLIOGRAPHY	65
AKNOWLEDGMENTS	66

Introduction and aim

The heart is a wonderful but complex organ: it uses electrochemical mechanisms in order to produce mechanical energy to pump the blood throughout the body and allow the life of humans and animals. This organ can be subject to several diseases and sudden cardiac death (SCD) is the most catastrophic manifestation of these diseases, responsible for the death of a large number of people throughout the world. It is estimated that 325000 [1] Americans annually die for SCD. SCD most commonly occurs as a result of reentrant tachyarrhythmias (ventricular tachycardia (VT) and ventricular fibrillation (VF)[2]) and the identification of those patients at higher risk for the development of SCD has been a difficult clinical challenge. Nowadays, a particular electrocardiogram (ECG) abnormality, “T-wave alternans” (TWA), is considered a precursor of lethal cardiac arrhythmias and sudden death, a sensitive indicator of risk for SCD [3-4]. TWA is defined as a beat-to-beat alternation in the shape, amplitude, or timing of the T-wave on the ECG, indicative of the underlying repolarization of cardiac cells [5]. In other words TWA is the macroscopic effect of subcellular and cellular mechanisms involving ionic kinetics and the consequent depolarization and repolarization of the myocytes. Experimental activities have shown that TWA on the ECG is a manifestation of an underlying alternation of long and short action potential durations (APDs), the so called APD-alternans, of cardiac myocytes in the myocardium [6]. Understanding the mechanism of APDs-alternans is the first step for preventing them to occur. In order to investigate these mechanisms it's very important to understand that the biological systems are complex systems and their macroscopic properties arise from the nonlinear interactions among the parts. The whole is greater than the sum of the parts, and it cannot be understood only by studying the single parts. In this sense the heart is a complex nonlinear system and its way of working follows nonlinear dynamics; alternans also, they are a manifestation of a phenomenon typical in nonlinear dynamical systems, called “period-doubling bifurcation”. Over the past decade, it has been demonstrated that electrical alternans in cardiac tissue is an important marker for the development of ventricular fibrillation and a significant predictor for mortality. It has been observed that acute exposure to low concentration of calcium does not decrease the magnitude of alternans and sustained ventricular Fibrillation (VF) [7] is still easily induced under these condition. However with prolonged exposure to low

concentration of calcium, alternans disappears, but VF is still inducible. This work is based on this observation and tries to make it clearer. The aim of this thesis is investigate the effect of hypocalcemia spatial alternans and VF doing experiments with canine hearts and perfusing them with a solution with physiological ionic concentration and with a solution with low calcium concentration (hypocalcemia); in order to investigate the so called memory effect, the experimental activity was modified during the way. The experiments were performed with the optical mapping technique, using voltage-sensitive dye, and a custom made Java code was used in post-processing. Finding the Nolasco and Dahlen's criterion [8] inadequate for the prediction of alternans, and taking into account the experimental results, another criterion, which consider the memory effect, has been implemented. The implementation of this criterion could be the first step in the creation of a method, AP-based, discriminating who is at risk if developing VF. This work is divided into four chapters: the first is a brief presentation of the physiology of the heart; the second is a review of the major theories and discovers in the study of cardiac dynamics; the third chapter presents an overview on the experimental activity and the optical mapping technique; the fourth chapter contains the presentation of the results and the conclusions.

BIBLIOGRAPHY

- [1] R.L. Verrier, K. Kumar, and B.D. Nearing Basis for sudden cardiac death prediction by t-wave alternans from an integrative physiological perspective. *Heart Rhythm* 6: 416-422 (2009).
- [2] D. Zipes, and J. Jalife. *Cardiac Electrophysiology: From Cell to Bedside*. Philadelphia: Saunders (2004).
- [3] D. S. Rosenbaum, L.E. Jackson, J. M. Smith, H. Garan, J. N. Ruskin, R. J. Cohen. Electrical alternans and vulnerability to ventricular arrhythmias. *N. Engl. J. Med.* 330: 235-241 (1994)
- [4] S. Narayan. T-wave alternans testing for ventricular arrhythmias. *Prog. Cardiovasc. Dis.* 51: 118-127 (2008).
- [5] S. Narayan. T-wave alternans and the susceptibility to ventricular arrhythmias. *J. Am. Coll. Cardiol.* 47: 269-281 (2006).
- [6] J. M. Pastore, S. D. Girouard, K. R. Laurita, F. G. Akar, and D. S. Rosenbaum. Mechanism linking t-wave alternans to the genesis of cardiac fibrillation. *Circulation* 99: 1385-1394 (1999).
- [7] M. L. Riccio, F. Hua, D. J. Lomonte, K. R. Venator, S. Cerda-Gonzales, and R. F. Gilmour, Jr. Effects of Hypocacemia on electrical restitution and Ventricular Fibrillation. *31st Annual International Conference of the IEEE EMBS* Minneapolis, Minnesota, USA (2009).
- [8] J. B. Nolasco, and R. W. Dahlen. A graphic method for the study of alternation in cardiac action potentials. *J. Appl. Physiol.* 25, 191–196. 1968.

1. The heart: anatomy and physiology

The heart plays a very important role in the life of a living being pumping blood throughout the body; in the following a description of its anatomy and functions will be presented.

1.1 The Heart

The heart is a muscle and even though it is a striated muscle actually it is an involuntary muscle. It is shaped like an inverted pyramid and is contained in the center of the rib cage. Located between the lungs and surrounding the diaphragm, it is separated by esophagus and aorta from the vertebral column and it is protected by sternum and rib cartilages. The heart is enclosed in double-walled membrane called pericardium which is made up by two layers: a superficial one, fibrous pericardium, and the inner one, serous pericardium. It envelops, lines and protects the whole contracting organ, anchoring its surrounding structures, preventing excessive dilation and limiting ventricular filling. The pericardial cavity, the space between the two layers, is filled with 10 ÷ 50 ml of fluid [1], the pericardial fluid; this reduces the friction caused by the beating and moving of the heart. The human heart is divided into four chambers communicating two by two: left atrium (LA) and left ventricle (LV), the so called left heart; and right atrium (RA) and right ventricle (RV), known as the right heart. Four valves ensure the selective and unidirectional flow: two between the atria and the corresponding ventricles and two between the ventricles and the big arteries: mitral and tricuspid valves control the atrioventricular (AV) communication, while aortic and pulmonary valves, semilunar (SL), regulate the outflow in the arteries leaving the heart. Papillary muscles, together with chordae tendons synchronously act with fluid pressure as an external trigger in order to regulate the correct blood flow between the chambers (see fig.1). From a functional point of view, the heart can be regarded as two parallel synchronized pumps separated by a septum: from the right atrium, the blood flows through the tricuspid valve to the right ventricle. Here, it is pumped out of the pulmonary semilunar valve through the pulmonary artery to the lungs. From there, blood flows back through the pulmonary vein to the left atrium. Then it travels through the mitral valve to the left ventricle, from where it is pumped through the aortic semilunar valve to the aorta and to

the rest of the body. The (relatively) deoxygenated blood finally returns to the heart through the inferior vena cava and superior vena cava, and enters the right atrium where the process began. The heart sounds, auscultated with a stethoscope, are actually the sounds of the valves flapping closed. During an heart cycle, the AV valves close first followed by the semilunar valves. The different contractile functions of the four chambers motivates the differences in their tissue properties, which assume a more durable and thicker wall structure for ventricles than for atria.

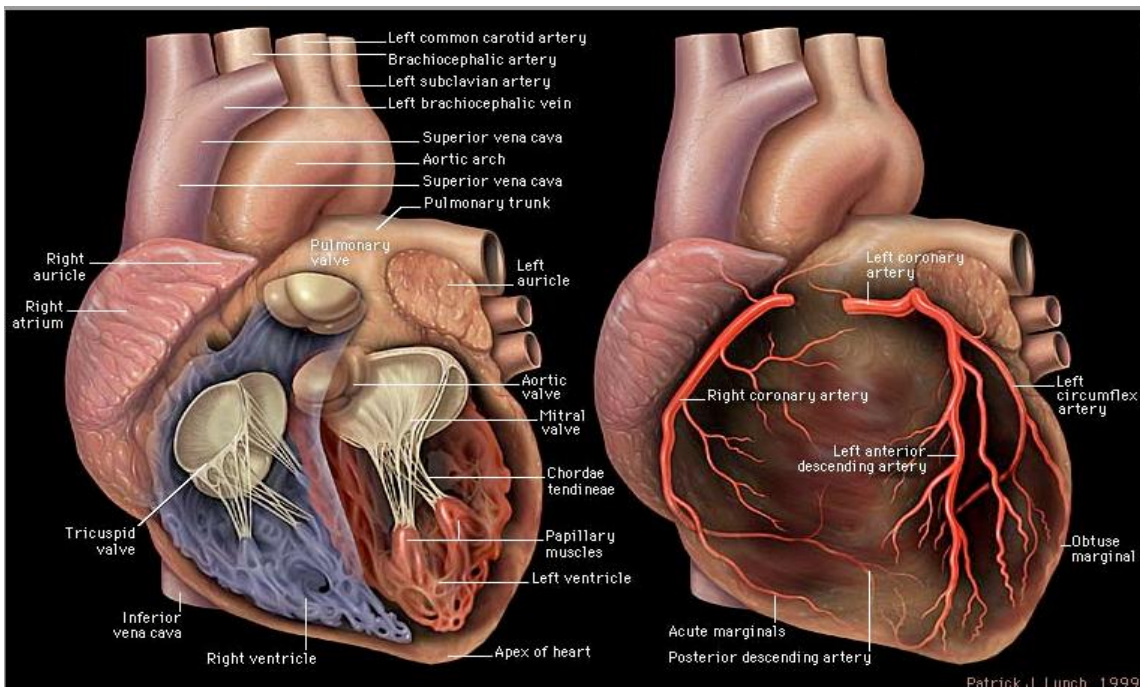
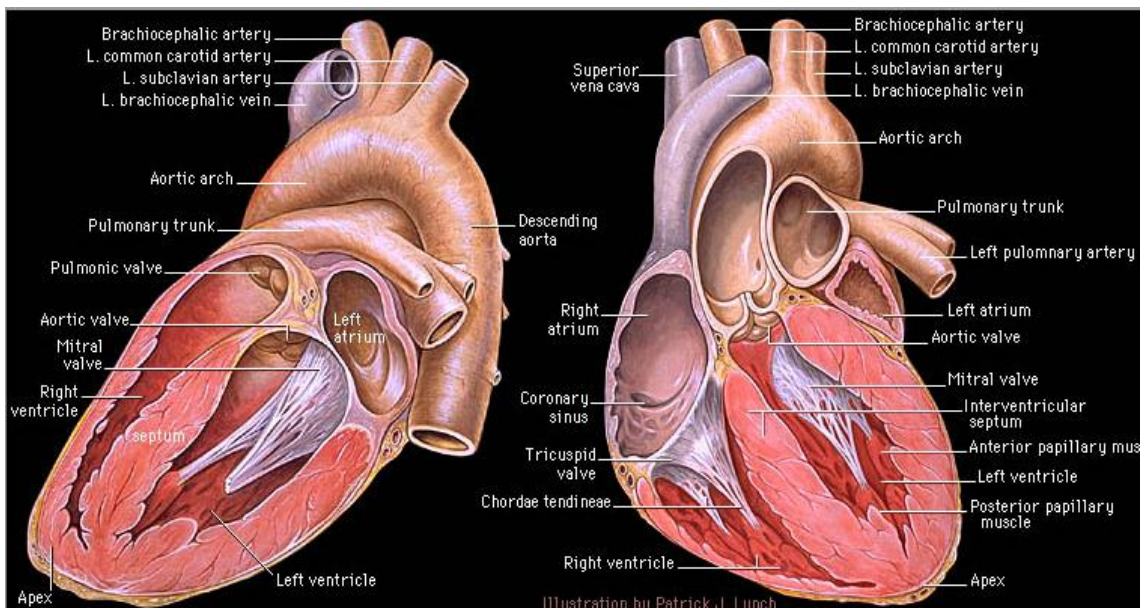


Figure 1: Gross anatomy of the heart [2]: (TOP) sectional view from both left and right side. (BOTTOM) three-dimensional view of the internal structures and of the coronary complex.

Cardiac wall tissue is composed of three layers: epicardium, the outer layer, myocardium, the middle layer, and endocardium, the inner layer which comes directly into contact with blood [3]. The cardiac muscle is usually described as a syncitium. It consists of densely packed cells, the cardiac myocytes, organized in fiber-like arrays, the cardiac fibers [4]. Each single myocyte is roughly cylindrical in shape with typical dimensions of $30\div 100\ \mu\text{m}$ in length and $8\div 20\ \mu\text{m}$ in diameter. Each cell is enclosed in its double layered phospholipidic membrane, fundamental for the maintenance of its intracellular state. Cardiac cells are surrounded by the interstitial fluid and are separated one from the others with exception of the limited regions where two adjacent membranes are melted, the so called gap junctions (fig.2). Such structures allow a single cell to be connected to as many as ten other cells, thus forming the cardiac fibers. The presence of gap junctions can explain the structural electrical anisotropy typical of cardiac cells and fibers: because of the low conductance of the membrane and the regional organization of the connexines in proximity to the ends of the cell, the ionic currents encounter an easier path in the longitudinal direction than in the orthogonal one to the main axis of the cell. Therefore, the resulting mean electrical conductivity is much higher in the direction of the fiber [5]. Throughout the whole heart, the fibers usually form layers or sheets with different radial orientations with respect to the ventricular surface. The rotational angle from epicardium to endocardium can reach 180° . Obviously, this is not generally true, in fact, in the subepicardial region this angle is $\sim 90^\circ$, in order to be tangent to the epicardial surface itself [6, 7], while into the ventricular wall it is $\sim 120^\circ$ with parallel sheets to both epicardium and endocardium surfaces. Such a complex structure induces a rotational propagation direction to the ionic current, as evidenced in the following.

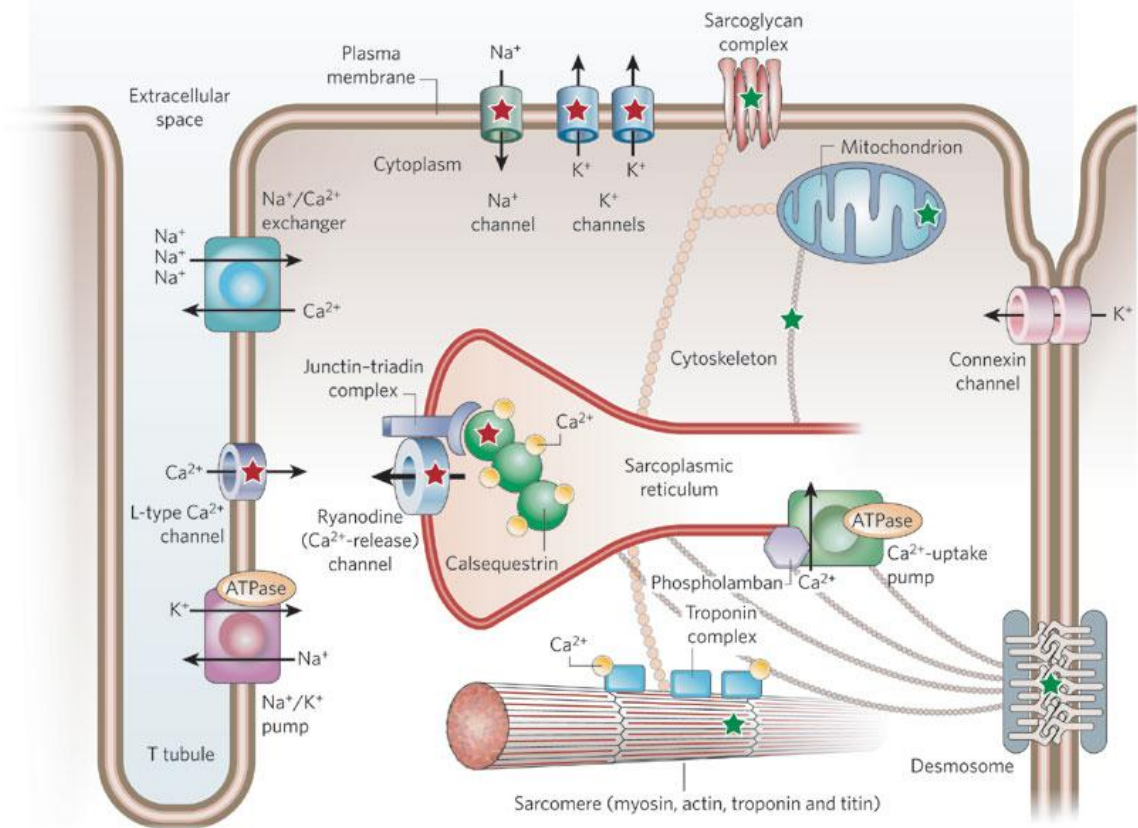
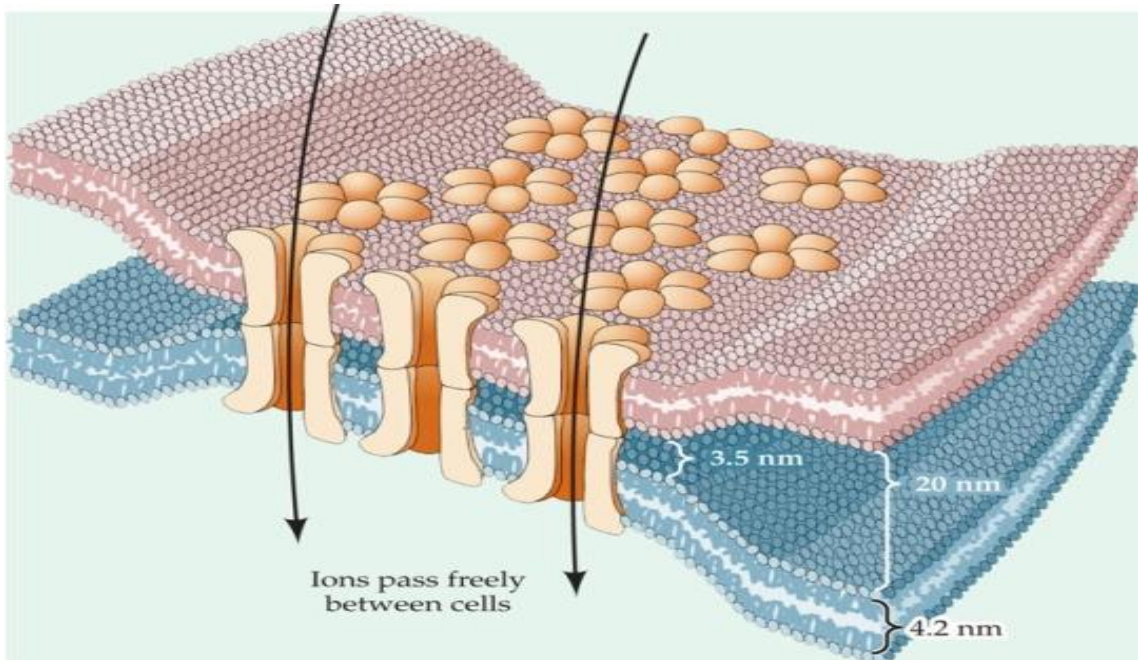


Figura 2: (TOP) Gap junctions between two cells (modified from [8]). (BOTTOM) Schematic representation of cardiac cell membrane protein structures and end processes (gap junctions) [9]; it's possible to notice the invaginations of the cell membrane, the transverse tubular system.

1.1.1 Electrical activity and propagation

In fig.3 a schematic representation of the differentiated muscular cells for fast action potential conduction and the electrical pathways are shown; At the macroscopic level, the spread and propagation of the electrical activation in the heart appears smooth, continuous and uniform.. With the term depolarization, it is intended the firing of the cardiac cells, initiating or continuing an impulse. With the term repolarization, it is intended the regenerating of the cardiac cells, while the cell is not firing, but building up the energy to depolarize again. In brief:

- The sinoatrial or SA node, located in the right atrium at the superior vena cava, consists of specialized self-excitatory muscle cells, pacemaker cells, generating an action potential at the rate of about $60 \div 100$ bpm. From the SA node, activation propagates throughout the atria reaching the AV node.
- The atrioventricular node or AV node, located at the boundary between the atria and ventricles just superior to the atrioventricular septum, is again self-excitatory at the rate of about $40 \div 60$ bpm, but, receiving the SA node activation, it follows this higher frequency. The AV node provides the only conducting path from the atria to the ventricles.
- The bundle of His is a specialized conduction system providing propagation from the AV node to the ventricles. Distally, it separates into two bundle branches propagating along each side of the septum. More distally the bundles ramify into the Purkinje fibers that diverge to the inner side of the ventricular wall and support an high propagation speed. These have an intrinsic rate of $20 \div 40$ bpm.
- From the inner side of the ventricular wall, the many activation sites cause the formation of a wave front which propagates through the ventricular mass toward the outer wall. The duration of the action impulse is much shorter at the epicardium than at the endocardium, the termination of activity appears as if it were propagating from epicardium toward the endocardium.

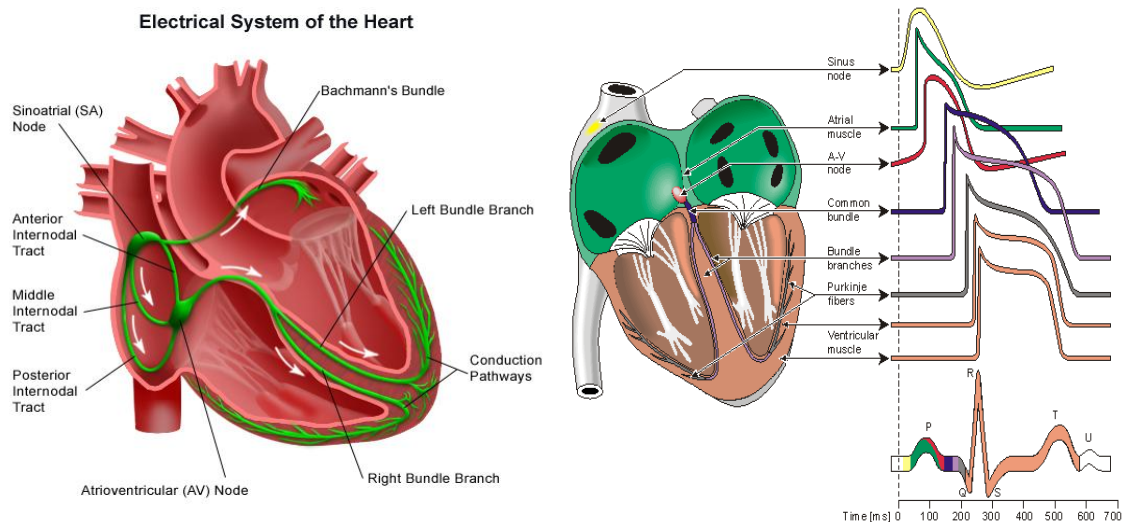


Figure 3. (LEFT) Cardiac activation network, pathways from atria to ventricles [10]. (RIGHT) Action potentials morphology at the different levels of the activation network [11].

Since the intrinsic rate of the SA node is the highest, it sets the activation frequency of the whole heart. If the connection from the atria to the AV node fails, the AV node adopts its intrinsic frequency. If the conduction system fails at the bundle of His, the ventricles will beat at the rate determined by their own region that has the highest intrinsic frequency. However, at cellular level, this spread exhibits small delays on the gap junctions depending on the conditions surrounding the cell membrane [12]. In fact, the conductance of these junctions assumes a comparable value to that of the entire intracellular region within a cell [13]. As said before, the Purkinje specialized conduction system allows the action potential signal to propagate at speeds of meters per second: such a feature allows a rapid excitation of the ventricles in a synchronized manner thus producing an effective contraction. The synchronization of ventricular contraction, is often involved in ventricular arrhythmias in various ways.

1.2 Excitation-contraction coupling

There is a steady potential difference across the ventricular cell membrane that is almost of the same size as the equilibrium potential for potassium ions, K^+ (-94mV), that is -90mV (see fig.4). This negative potential is referred to as the resting membrane potential (RMP), because it represents the potential difference across the cell membrane (inside negative) at rest between successive action potentials.

1.2.1 Action potentials: phases

The action potential starts when electrochemical forces favor the abrupt influx of Na^+ from neighboring regions. The amplitude of an action potential is independent of the amount of current that produced it. In other words, larger currents do not create larger action potentials: when the depolarization reach the threshold of about -40 mV , from -90 mV , action potentials occur. Therefore, action potentials are said to be all-or-none signals, since either they occur fully or they do not occur at all. An action potential can be divided in five phases:

- Phase 0 (Rapid depolarization): the abrupt upstroke, due to the rapid entry of Na^+ into the cell, is responsible of the fast depolarization. At about $+30\text{mV}$ the fast Na^+ -channels become voltage-inactivated because of the closure of inactivation gates and the Phase 0 ends.
- Phase 1 (Initial repolarization): it is the early repolarization from the upstroke depending on the K^+ - outflow.
- Phase 2 (Plateau phase): the slow Ca^{2+} channels remain open for a long period, up to 300ms. Ca^{2+} activates the muscle contractile process. Plateau occurs because the Ca^{2+} inflow matches the K^+ outflux.
- Phase 3 (Repolarization): it is the terminal repolarization. At the very end of the plateau the slow channels close, the permeability for K^+ increases rapidly and a large amount of K^+ go out of the ventricular fibers. The equilibrium potential is rapidly approached.
- Phase 4 (Resting potential): it is recognized by a RMP of -90 mV . The Na^+ - K^+ pump restores ionic concentrations in a ratio of 3:2.

Phase 4 is referred as relative refractory period: enough of the fast Na^+ -channels are recovered, so that a sufficiently large stimulus can break through and produce an action

potential although smaller than normal. Once an action potential starts there is a period, from Phase 0 to half of Phase 3, called effective refractory period (ERP), where a new action potential cannot be initiated. As a consequence, no stimulus is sufficient to trigger contraction regardless of size. The ERP acts as a protective mechanism in the heart by preventing multiple, compounded action potentials from occurring.

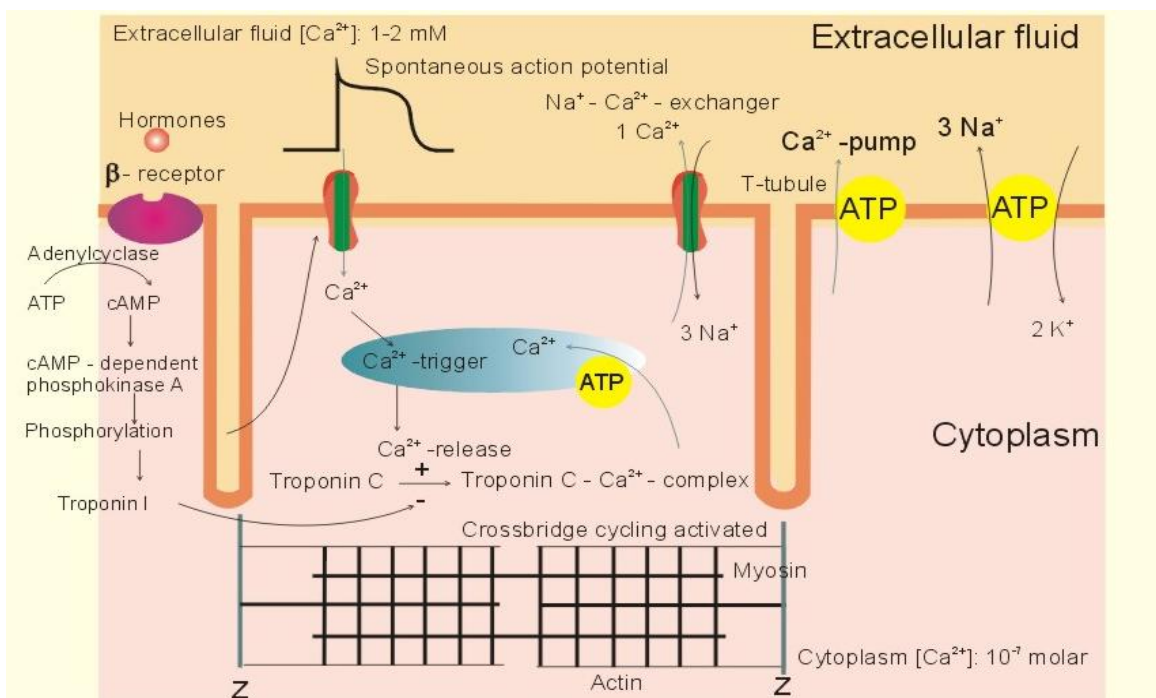
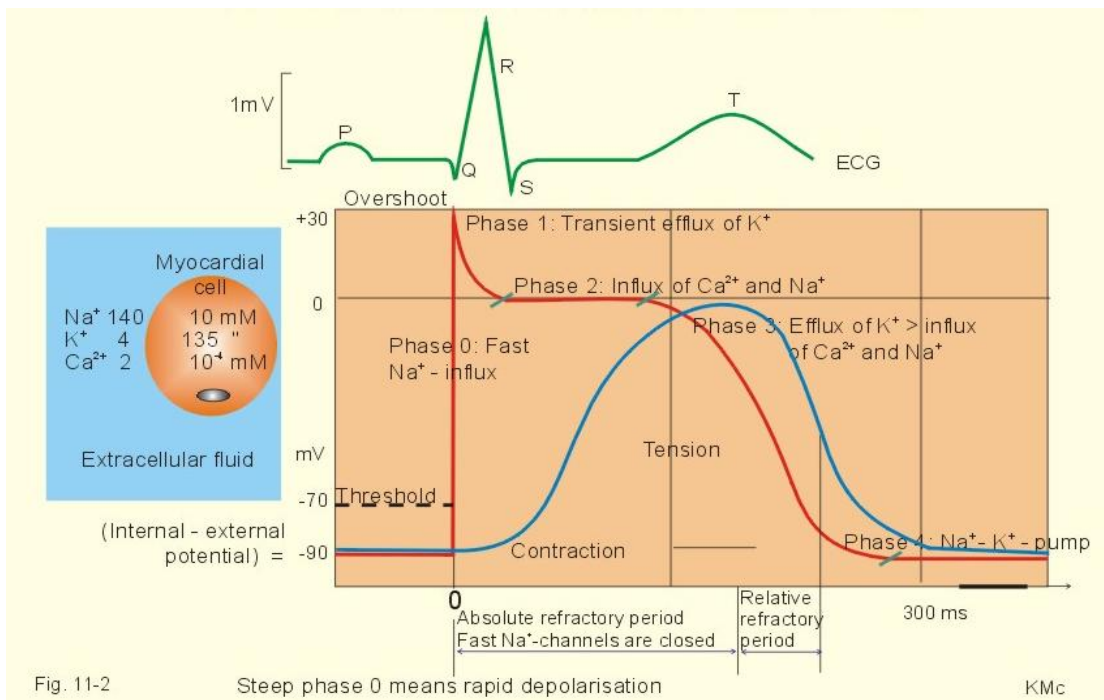


Figure 4. Excitation-contraction waves [14]. (TOP) Recordings of ECG (above), intracellular membrane potential (red curve) and contraction (blue curve) of one heart cycle in a ventricular fiber. Action potential phases description. (BOTTOM) Sub-cellular mechanisms of excitation-contraction coupling in a cardiac cell.

1.2.2 Subcellular mechanisms: calcium cycle

The mechanism for muscle contraction is based on the so called excitation-contraction coupling (see fig.4), which links electric action potential to muscular movement through subcellular triggering. Calcium ions, from the extracellular medium and from the sarcoplasmic reticulum (SR), are the main actors in cellular contractility and moreover critical both in the mechanical dysfunction and arrhythmogenesis associated with congestive heart failure [15]. A detailed control of calcium cycling requires an integrated approach in which several systems are considered [16, 17]. A schematic view of the calcium dynamics in the exciting-contraction coupling is the following:

- L-type Ca^{2+} channels are activated during the cardiac action potential;
- Ca^{2+} enter the cell through the L-type Ca^{2+} channels and Sodium-Calcium exchange (NCX);
- Entry of the calcium in the cell activates a mechanism called Calcium induced calcium release (CICR): Ca^{2+} from the outside triggers the release of the Ca^{2+} from the sarcoplasmic reticulum (SR) making the ryanodine channels open;
- CICR raises cytosolic free Ca^{2+} , causing calcium binding to multiple buffers, and mainly with the protein troponin C (TnC);
- when Ca^{2+} binds to TnC, it switches on the myofilaments in a cooperative manner activating the contractile apparatus (the sarcomere) (fig. 2)
- Calcium ions are pumped back into the SR, causing cellular relaxation and forcing muscle contraction to cease: mainly four calcium transporters are used to remove Ca^{2+} from the cytosol: SR Ca^{2+} -ATPase, sarcolemmal NCX, sarcolemmal Ca^{2+} -ATPase, and mitochondrial Ca uniporter.

1.3 Cardiac cycle

Through the centuries several devices were invented, adapted and used in measuring the activities of the human heart. In fig. 5 (Top) are shown the curves obtained using different technologies such as ECG and phonogram of the human subject. Through these analyses, characteristic volumetric ranges of the healthy heart were standardized:

1. 110 ÷ 120 ml for end-diastolic volume (EDV): it is the volume of blood in the right and/or left ventricle during the phase of end load or filling in (diastole);

2. 40 ÷ 50 ml for end-systolic volume (ESV): it determines the stroke volume, that is the output of blood pumped by the heart during a single phase of the cardiac cycle.
3. 70 mL for the stroke volume (SV): is the volume of blood pumped from one ventricle of the heart with each cardiac cycle.
4. 60% for ejection fraction (Ef): it is the fraction of blood pumped out (forward) from the right ventricle of the heart to the pulmonary circulation (lungs) and from the left ventricle of the heart to the systemic circulation (brain and body) during each cardiac cycle.

On such bases, other indicators were introduced, i.e. the stroke work output (amount of energy converted to work during a heartbeat), that is defined as the pressure difference between veins and arteries, and kinetic energy of blood flow (see fig. 5 (Bottom)) the volume pressure diagram). This allows a direct visualization of the four phases as:

1. Period of filling.
2. Period of isovolumic (isometric) contraction.
3. Period of ejection.
4. Period of isovolumic relaxation.

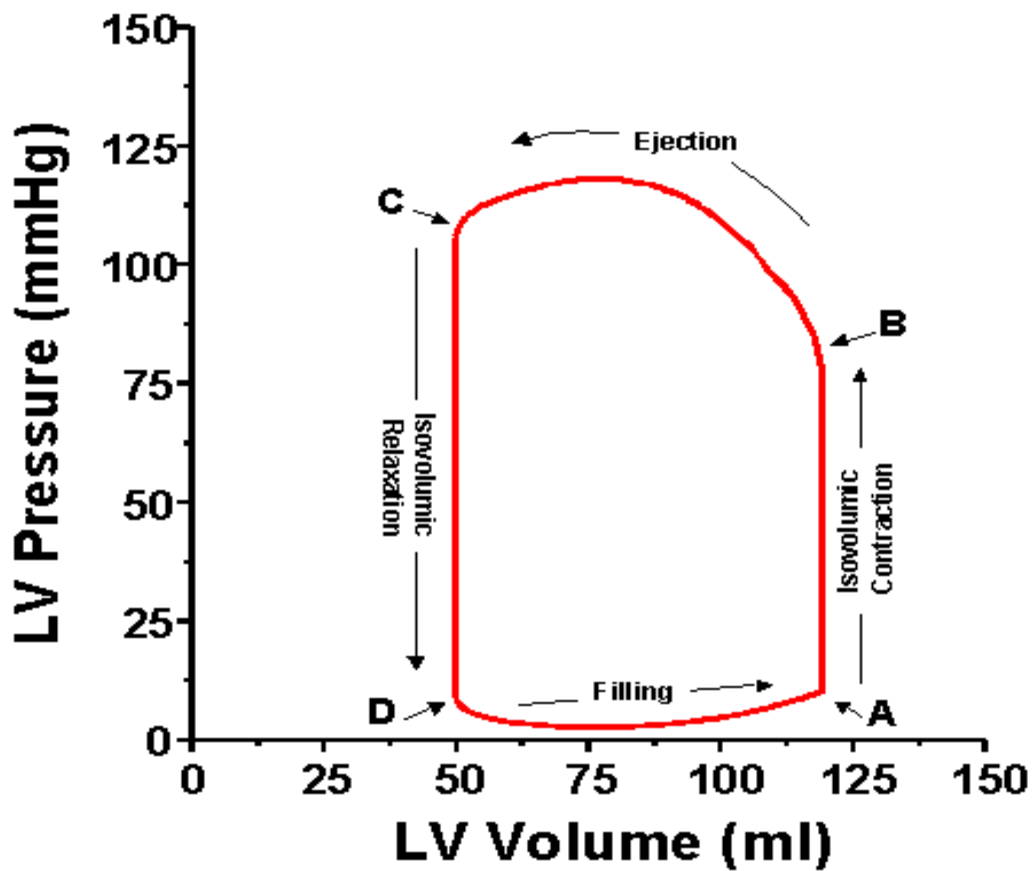
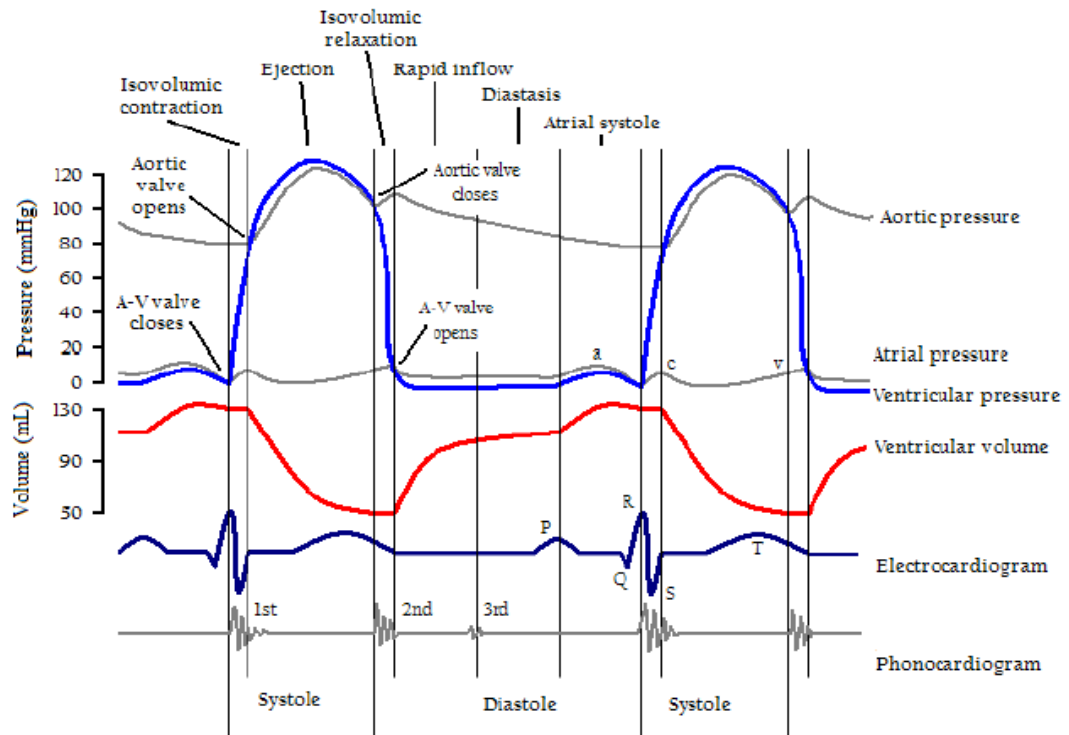


Figure 5. (TOP) Cardiac cycle curves of volume, pressure and ECG [18]. (BOTTOM) Volume-Pressure diagram of cardiac cycle with phase identification [19].

1.4 Cardiac arrhythmias

Cardiovascular diseases are the leading causes of death in most developed countries [20]. The effects of the mechanisms of arrhythmogenesis and arrhythmia termination on cardiac electrical activity has been studied following multidisciplinary approaches: this has allowed an improvement of pharmacological and electrical therapies [21], thus discovering and creating new technologies and theories [22]. The difficulty or impossibility to measure all the quantities of interest in vivo is still an open problem and researchers are obliged to relate in vitro measurements, performed on small tissue preparations or isolated cells, to the dynamics of the entire heart. Several mechanisms have been related to cardiovascular diseases and cardiac arrhythmias.

1.4.1 Arrhythmias: definition and classification

The term arrhythmia describes the wide set of abnormal electrical activity of the heart: the cardiac rhythm may be faster or slower, and regular or irregular as well. The most dangerous cardiac arrhythmias are due to reentrant waves that recirculate through the tissue with a higher frequency than the one of the heart's natural pacemaker. The corresponding literature targets this phenomenon as "rotating spiral waves". The onset of cardiac arrhythmias was associated with the concept of reentry by McWilliam for first at the end of the 19th century [23]: differences in action potential conduction and in the duration of the so called refractory periods in myocardial fibers can help the formation of waves which "reenter" inducing a re-excitation of previously excited tissue. The wrong behavior of the Purkinje plays has an important role in the development of arrhythmic pathologies [24]. In fact, this network can act as a source of triggering activities [25-26] such as focal and post-shock activations [27], or as part of reentrant circuits [28]. Cardiac arrhythmias are divided into two main groups and classified as [29]:

1. Disorders of rhythmogenesis:

- (a) In the sinus node: sinus tachycardia (heart rate above 100 bpm), sinus bradycardia (heart rate below 60 bpm) or sinus arrhythmia (rise in heart rate during inspiration followed by a fall during expiration).
- (b) Outside the node: ectopic beats (pacemaker cells outside the sinus node), tachycardia (paroxysms), and fibrillation (tumultuous twitching of ventricular

muscle fibre) and shifting pacemaker (the impulse originates in shifting locations inside the SN, or the pacemaker shifts from the SN to the AV-node).

2. Conduction abnormalities (cardiac block):

- (a) Sinoatrial block: long intervals between consecutive P-waves.
- (b) Atrioventricular block: blockage of the conduction from the atria to the AV-node.
- (c) Bundle branch block: block of the right or the left bundle branches.
- (d) WPW-syndrome: Wolf-Parkinson-White block is not a direct block of the conduction through the Hiss bundle and branches, but is caused by a short cut through an extra conduction pathway from the atria to the ventricles.
- (e) Long QT-syndrome: frequently a genetic condition, where fast repolarized cells are re-stimulated by cells that have not repolarized.

1.4.2 Anatomical and functional reentry

As previously said, reentrant waves are probably the main cause of lethal arrhythmias. Commonly the medical literature refers to two kinds of reentry: anatomical reentry (AR) and functional reentry (FR). The former is connected with topological properties of cardiac tissue, in fact they occur whenever unexcitable obstacles are present into the tissue (i.e. scars due to an infarct) and the electrical wave can rotate around; the latter, related to the local heterogeneity of the tissue, does not necessitate of such anatomical conditions, in fact the electric wave itself is responsible of a reduced excitability of the medium, thus creating a so called functional block around which the wave periodically rotates around. Experimental and modeling examples of AR and FR are shown in fig. 6. The conditions for an AR to occur is related to the perimeter of the obstacles in the cardiac tissue. [30-32].

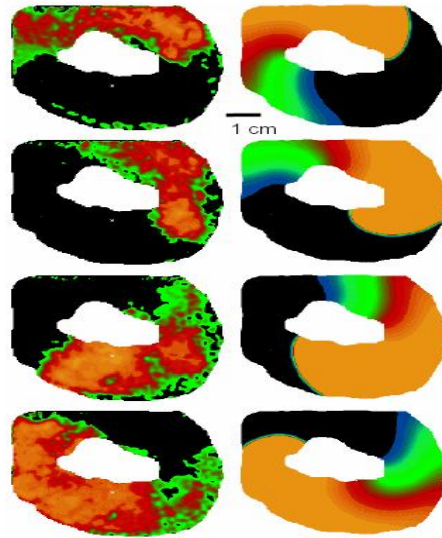


Figure 6: Reentry. Experimental and simulated examples of an anatomical reentrant arrhythmia. On the left column: optical mapping recording of goat right ventricle preparation; the central region, serving as an obstacle, has been cryoablated. On the right column: two-dimensional representation of the experimental geometry through phenomenological numerical simulations of cardiac tissue (adapted from [30]).

On the one hand anatomical reentry results particularly important in the atria and the corresponding pathology has been known clinically since 1920s as atrial flutter [33]. Atrial tissue includes different structures such as large blood vessels and valve annuli of different sizes. Each of them can represent an obstacle around which activation waves can strongly circulate. On the other hand, functional reentry is even more dangerous because it can appear on healthy tissues too. Under normal conditions, as often observed in vitro preparations, atrial arrhythmias do not occur spontaneously and usually self-terminate quickly if initiated. In ventricular tissue, on the contrary, reentrant waves can be initiated and sustained readily in large hearts (i.e. there is a sort of critical mass). The physiological condition, however, is strongly altered in the presence of pharmacological agents or cardiovascular diseases.

1.5 Clinical treatments for arrhythmias

Ventricular fibrillation is a lethal arrhythmia: the unsynchronized contraction of the ventricles doesn't allow the heart to pump blood. That's the reason why it must be terminated rapidly to prevent death and/or to minimize damage to cardiac tissue and other organs. Termination of ventricular arrhythmias is indicated in the medical literature as well as in the clinical practice as defibrillation. Atrial arrhythmias in healthy atria, on the other hand, are an exception and atrial fibrillation is characteristic of diseased tissues. Even though less dangerous than ventricular fibrillation, such arrhythmias definitively increase the risk of other cardiac problems, including stroke

and ventricular fibrillation itself. Termination of atrial arrhythmias is called cardioversion. Arrhythmia termination generally is accomplished either through electrical stimulation, resetting electrical activity directly, or through pharmacological therapy, that affect the underlying dynamics modifying the electrophysiological properties of the tissue. Sometimes ablations, surgical lesions of tissue, created to disrupt reentrant pathways, are adopted in terminating certain types of arrhythmias: some forms of ventricular tachycardia, atrial fibrillation and atrial flutter.

BIBLIOGRAPHY

- [1] S. Ben-Horin, A. Shinfeld, E. Kachel, A. Chetrit, and A. Livneh. The composition of normal pericardial fluid and its implications for diagnosing pericardial effusions. *Am. J. Med.* 118:636-40, 2005.
- [2] www.yale.edu
- [3] E. Drouin, F. Charpentier, C. Gauthier, K. Laurent, and H. Le Marec. Electrophysiologic characteristics of cells spanning the left ventricular wall of human heart: evidence for presence of M cells. *JACC.* 26:185-192, 1995.
- [4] R. Sommer, and B. Scherer. Geometry of cell and bundle appositions in cardiac muscle: light microscopy. *Amer.J. Physiol.*, 248:H792-H803, 1985.
- [5] L. Clerc. Directional differences of impulse spread in trabecular muscle from mammalian heart. *J. Physiol.* 25:335-346, 1976.
- [6] P. M. F. Nielsen, I. J. Le Grice, B. H. Smaill, and P. J. Hunter. Mathematical model of geometry and fibrous structure of the heart. *Amer. J. Physiol.* 29:H1365-H1378 (1991).
- [7] D. Streeter. *Gross morphology and fiber geometry of the heart*, in Handbook of Physiology: The Cardiovascular System, S. R. Geiger, Ed. Bethesda.
- [8] <http://www.mindsmachine.com>
- [9] B.C. Knollmann and D.M. Roden. A genetic framework for improving arrhythmia therapy. *Nature* 451: 929-936 (2008).
- [10] <http://www.lpch.org>
- [11] <http://www.bem.fi>.
- [12] R. Weingart, and P. Maurer. Action potential transfer in cell pairs isolated from adult rat and guinea pig ventricles. *Circ. Res.* 63:72 (1988)
- [13] R. Weingart. Electrical properties of the nexal membrane studied in rat ventricular pairs. *J. Physiol. (London)*. 370:267 (1986).
- [14] P. E. Paulev, and G. C. Zubieta. *Textbook in Medical Physiology And Pathophysiology Essentials and clinical problems*. 2nd Edition, Copenhagen, Denmark (2000).
- [15] D. M. Bers. Calcium Fluxes Involved in Control of Cardiac Myocyte Contraction. *Circ. Res.* 87:275-281 (2000).

- [16] M. J. Berridge, M. D. Bootman, and H. L. Roderick. Calcium signalling: dynamics, homeostasis and remodelling. *Nature Rev.* 4:517-529 (2003).
- [17] D. A. Eisner, H. S. Choi, M. E. Díaz, S. C. O'Neill, and A. W. Trafford. Integrative analysis of calcium cycling in cardiac muscle. *Circ Res.* 87:1087-1094 (2000).
- [18] <http://en.wikipedia.org>.
- [19] <http://ccnmtl.columbia.edu/projects/heart/exercises/MechPropHeart/lecture.html>
- [20] R. Mhera. Global public health problem of sudden cardiac death. *J.Electrocardiol.* 40: S118-22. Review (2007).
- [21] C. S. Henriquez, and A. A. Papazoglu. Using computer models to understand the roles of tissue structure and membrane dynamics in arrhythmogenesis. *Proceed. IEEE*, 84:334-354 (1996).
- [22] S. Luther, F. H. Fenton, B. G. Kornreich, A. Squires, P. Bittihn, D. Hornung, M. Zabel, J. Flanders, A. Gladuli, L. Campoy, E. M. Cherry, G. Luther, G. Hasenfuss, V. I. Krinsky, A. Pumir, R. F. Gilmour Jr, and E. Bodenschatz. Low-energy control of electrical turbulence in the heart. *Nature.* 475:235-241 (2011).
- [23] J. A. McWilliam. Fibrillar contraction of the heart. *J. Physiol.* 8:296-310 (1887).
- [24] M. J. Janse, F. J. Wilms-Schopman, and R. Coronel. Ventricular fibrillation is not always due to multiple wavelet reentry. *J. Cardiovasc. Electrophysiol.* 6:512-521 (1995).
- [25] D. O. Arnar, and J. B. Martins. Purkinje involvement in arrhythmias after coronary artery reperfusion. *Am. J. Physiol. Heart Circ. Physiol.* 282:H1189-H1196 (2002).
- [26] F. Bogun, E. Good, S. Reich, D. Elmouchi, P. Igetic, D. Tschopp, S. Dey, A. Wimmer, K. Jongnarangsin, H. Oral, A. Chugh, and F. Pelosi, F. Morady. Role of Purkinje fibers in post-infarction ventricular tachycardia. *J. Am. Coll. Cardiol.* 48:2500–2507 (2006).
- [27] M. Haïssaguerre, D. C. Shah, P. Jaïs, M. Shoda, J. Kautzner, T. Arentz, D. Kalushe, A. Kadish, M. Griffith, F. Gaïta, T. Yamane, S. Garrigue, M. Hocini, and J. Clémenty. Role of Purkinje conducting system in triggering of idiopathic ventricular fibrillation. *Lancet.* 359:677-678 (2002).
- [28] D. J. Dossall, K. A. Cheng, J. Huang, J. S. Allison, J. D. Allred, W. M. Smith, and R. E. Ideker. Transmural and endocardial Purkinje activation in pigs before local myocardial activation after defibrillation shocks. *Heart Rhythm.* 4:758-765 (2007).
- [29] P. B. Tabereaux, G. P. Walcott, J. M. Rogers, J. Kim, D. J. Dossall, P. G. Robertson, C. R. Killingsworth, W. M. Smith, and R. E. Ideker. Activation patterns of Purkinje fibers during long-duration ventricular fibrillation in an isolated canine heart model. *Circ.* 116:1113-1119 (2007).
- [30] E. M. Cherry, and F. H. Fenton. Visualization of spiral and scroll waves in simulated and experimental cardiac tissue. *New J. Phys.* 10:125016, (2008).

- [31] E. M. Cherry, and S. J. Evans. Dynamics of human atrial cell models in tissue: restitution, memory, propagation, and reentry. *Prog. Biophys. Mol. Biol.* 98:24-37 (2008).
- [32] P. Comtois, and A. Vinet. Multistability of reentrant rhythms in an ionic model of a two-dimensional annulus of cardiac tissue. *Phys. Rev. E.* 72:051927 (2005).
- [33] S. D. Girouard, J. M. Pastore, K. R. Laurita, K. W. Gregory, and D. S. Rosenbaum. Optical mapping in a new guinea pig model of ventricular tachycardia reveals mechanisms for multiple wavelengths in a single reentrant circuit. *Circ.* 93:603-613 (1996).
- [34] T. Lewis, H. Feil, and W. Stroud. Observations upon flutter and fibrillation ii. Nature of auricular flutter. *Heart.* 7:127, 191-244 (1920).

2. Alternans and their role in cardiac arrhythmias

As it has been said before, alternans is a phenomenon developing at high heart rates. This mechanism occurs at different levels from the subcellular to the tissue one. The T-wave alternans (TWA) can be recorded using an ECG and is a manifestation of the alternans occurring to the lower levels. The following chapter focuses on electrical alternans or Action Potential (AP) alternans and also mathematical methods for their prediction will be introduced.

2.1 Alternans: definition and first concepts

In the previous chapter the Fig. 3 shows the action potential generated by different cells of the heart. Despite their differences in shape and timing each action potential period can be divided into two parts: the action potential duration APD which correspond to the systole and the diastolic interval DI corresponding to the diastolic phase of the heartbeat. Mathematically the APD is defined as the 90% (or 75%) recovery from the peak voltage. Generally set a voltage threshold the APD is the part above the threshold and the DI is the part below (fig. 7).

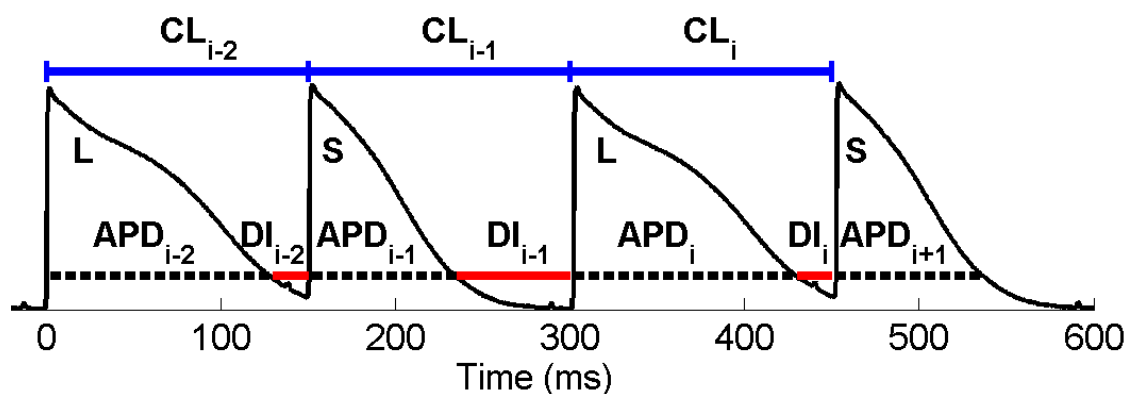


Figure 7. The APD (dotted lines) and the corresponding DI (red lines). The voltage corresponding to the horizontal line (dotted and red) is the voltage threshold.

AP alternans is an alternation of long and short APDs (and of short and long DIs respectively) despite a constant pacing period (CL in Fig. 7). Some experiments have shown that AP alternans are accompanied by concurrent alternations in amplitude of

intracellular Ca^{2+} transient (Ca^{2+} alternans) [1]. Given that AP alternans is linked to Ca^{2+} alternans, there are two hypothesis rising from this coupling:

- 1) AP alternans produces an alternation in the intracellular Ca^{2+} transient [2, 3];
- 2) Alternans in intracellular Ca^{2+} produces AP alternans [4, 5].

Despite this speculation, in this work, we focus on the AP alternans and his mathematical theory where the concept of restitution stands out.

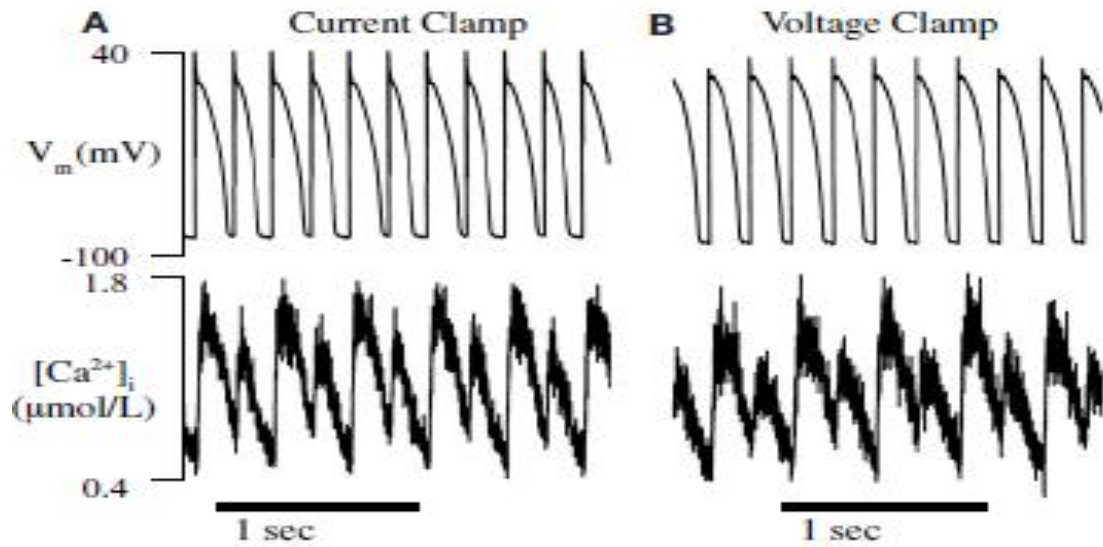


Figure 8. Alternans can be caused by intrinsic Ca^{2+} -cycling dynamics alone. The intracellular Ca^{2+} transients of paced (A) and AP clamped (B) isolated rabbit ventricular myocytes are observed using a fluorescent Ca^{2+} -sensitive dye (fura-2). (A) As expected, the APDs and Ca^{2+} transients of paced myocytes are seen to alternate from beat-to-beat when the cycle length is reduced to below a critical threshold (180ms). (B) The Ca^{2+} transients of AP clamped myocytes were still seen to alternate below approximately the same cycle length threshold as paced myocytes, in spite of fixed membrane voltage. This indicates that Ca^{2+} -cycling dynamics can alternate due to their own, intrinsic instability and has led many to conclude that Ca^{2+} -dynamics are solely responsible for cellular alternans [6].

2.2 The restitution relation

A consolidated analytical method for studying AP alternans is to plot the so called APD restitution relation [8, 7, 2]. The ADP restitution relation can also be used to predict the onset of alternans [8]. In according to Dr. Fenton and Dr. Cherry APD restitution “essentially describes a functional relationship between the duration of a cardiac action potential and the length of the quiescent interval (diastolic interval, or DI) preceding it.” [9]. Mathematically the APD restitution relation is:

$$APD_n = f(DI_{n-1}) \quad (I)$$

where f is the “functional relationship” between the APD_n and the DI_{n-1} . Another important mathematical relationship link the cycle length (CL) of each beat to the corresponding ADP ad DI:

$$CL_n = APD_n + DI_n \quad (II)$$

where CL is a constant (fig. 7). The APD restitution relation is obtained experimentally, using different experimental protocols, starting from the recording of the AP. In fig. 8 is shown an experimental APD restitution curve.

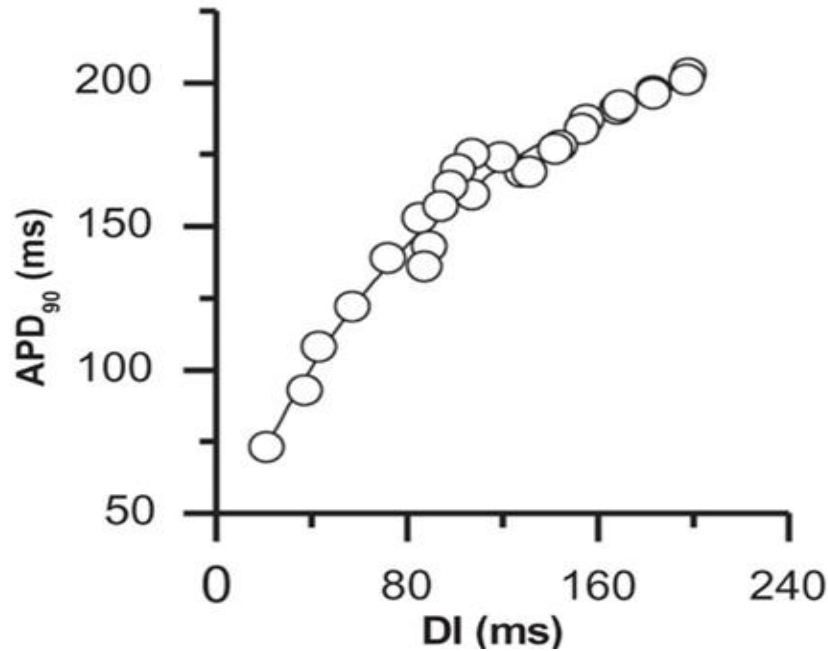


Figure 8. Experimental APD restitution curve from a rabbit (adapted from [11]).

Together with APD restitution relation also the conduction velocity (CV) restitution relation is relevant. The CV restitution relation is obtained plotting the CV versus the previous DI and it is very important as a mechanism of spatially discordant alternans (§ 2.4). Despite the simple definitions, the “real” APD restitution relation is more complicated: also cardiac memory (CM), due to the different timing of the ionic channels (Na, K⁺, L-Type Ca²⁺ channels) [10], and the presence of electrotonic effects influence APD restitution relation; thus, the APD restitution relation is actually a multivariable function.

2.2.1 The mechanism of APD alternans

Nolasco and Dahlen, first, in 1968 used a graphical method to show the occurring of APD alternans when:

$$|f'| = \left| \frac{df}{dDI_n} \right| > 1 \quad (III)$$

i.e. the slope of the APD restitution relation is greater than 1. Assuming no memory, the APD restitution relation is mathematically described as in (I + II). For each CL_n there is a fixed point and it can be determined by the intersection of the two curves. In fig. 9 there are two cobweb diagrams: on the left the slope of the restitution curve (a grey straight line) is smaller than 1 and the intersection between the gray line and the cyan one, satisfying the condition (II), is the fixed point where $APD = APD_s$ and $DI = DI_s$. At the beginning, at the point “1”, DI_1 and APD_2 , are far from the fixed point but after few iterations they approach the fixed point, eventually converging to it. In this case the equilibrium point is stable. The system develops transient alternans but, the less is the slope the faster alternans disappears. On the right of fig. 9 the case with slope greater than 1 is shown: alternans became bigger and bigger iteration after iteration until a 2:1 block occurs. The expression “2:1” means two electrical stimuli - one AP: the second stimulus doesn’t produce an AP because it occurs during the refractory period. In a similar way “1:1” means one stimulus- one AP, e.g. the sinus rhythm. Alternans is indicated using “2:2” which means that two different APs occur because of two equal stimuli.

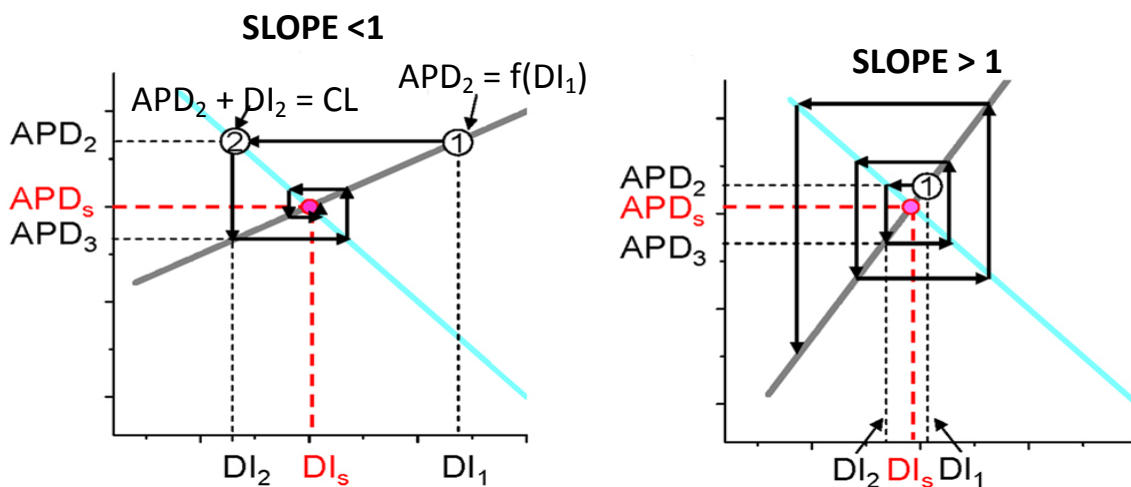


Figure 9. Cobweb diagrams: on the left the slope of the restitution curve is smaller than 1 and the fixed point is stable; on the right the slope is greater than 1 and the fixed point is unstable leading to permanent alternans and eventually to a conduction block.

Fig. 10 shows the same thing of fig. 9 but with a more realistic APD restitution curve. In A it's shown what happens if the CL is changed: in this case the fixed point red point at the new CL (blue line) is stable and after a little oscillation the system will reach the equilibrium; in B the system oscillate between long and short value of APDs and DIs it's a 2:2 condition; in C the system goes into a conduction block 2:1.

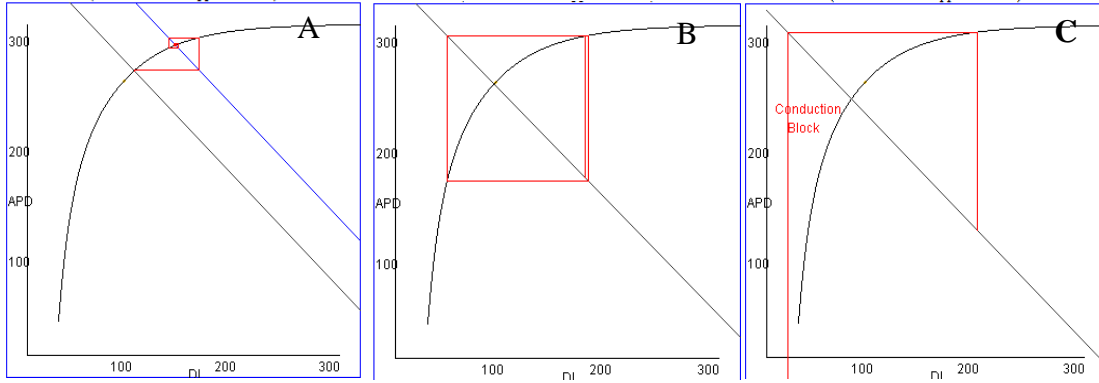


Figure 10. Three different situation of the system with a more realistic APD restitution curve [12].

The Nolasco and Dahalen's criterion seems to predict quite well the onset of APD alternans but it fails in other situations because of the more complicated nature of the APD restitution relation depending also on the CV, CM and electrotonic effects (see pag. 21).

2.2.2 Bifurcations

To describe the behavior of the system and to test the criterion suggested by Nolasco and Dahlen, the cobweb technique [13] is used; that is equivalent to consider the APD restitution relation like a one dimensional iterated map. Recalling the equations (I) and (II) , and substituting (II) into (I) it's easy to see that the APD restitution relation is an iterated map:

$$APD_n = f(CL - APD_{n-1}) \quad (IV)$$

The present APD depends on the previous APD (CL is a constant parameter experimentally imposed) by a non linear function f . Such a system is, mathematically speaking, a discrete dynamical system. These systems have some interesting properties that can be found in any text of nonlinear dynamics [13, 14]. Here only the bifurcations will be briefly presented as alternans is a manifestation of this property.

What is a bifurcation? Accordingly to several authors a bifurcation of a nonlinear dynamical system is a qualitative change in its dynamics obtained by varying parameters (fig.11). To be more specific a bifurcation occurs when, varying some

parameters, the phase portrait of a dynamical system changes its topological structure (e.g., the number of fixed points or close orbits).

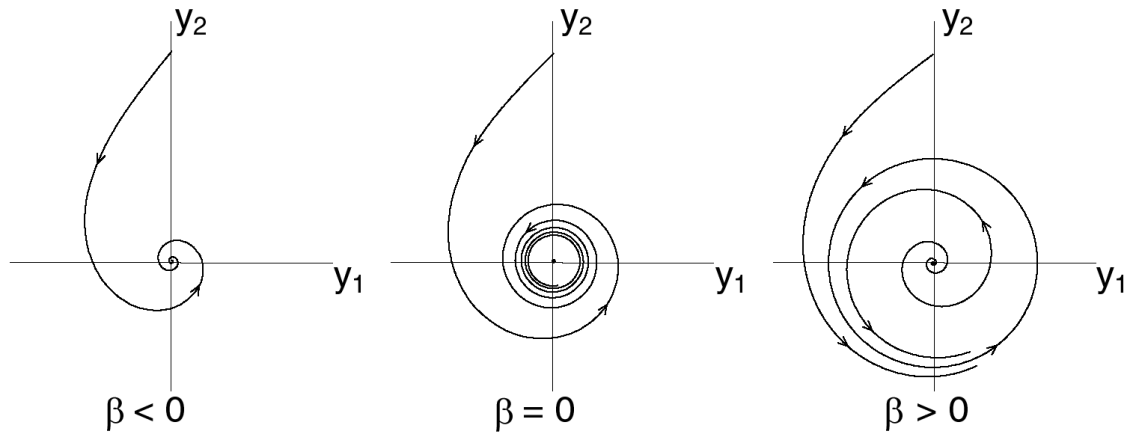


Figure 11. Supercritical Andropov-Hopf bifurcation in the plane. This bifurcation occurs in continuous dynamical systems: The dynamical system is described by the varying parameter β . The phase portrait changes from left to right: the point $(y_1, y_2) = (0, 0)$ is a stable focus ($\beta < 0$), a stable circle limit ($\beta = 0$) and an unstable focus surrounding by a stable circle limit.

One of the most occurring bifurcation in discrete dynamical system is the so called period-doubling bifurcation where the system switches to a new behavior with twice the period of the original system (fig. 12).

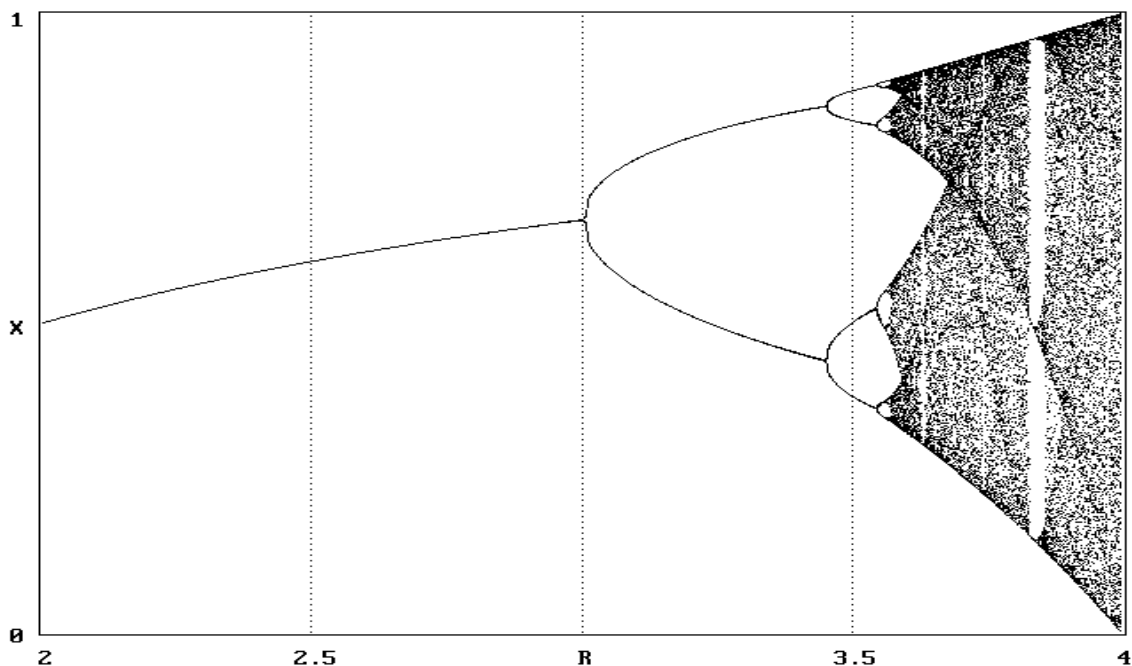


Figure 12. Bifurcation diagram. It describes the behavior of a discrete system as a function of the bifurcation parameter R . The system goes through several period doubling bifurcations while R becomes greater and greater.

Changing the parameters the system can go through several bifurcation and eventually reaching a more complex chaotic dynamics. Such a similar behavior is exhibited by cardiac myocytes: changing the CL (which is a parameter) it is possible to build a bifurcation diagram similar to that shown in fig. 12.

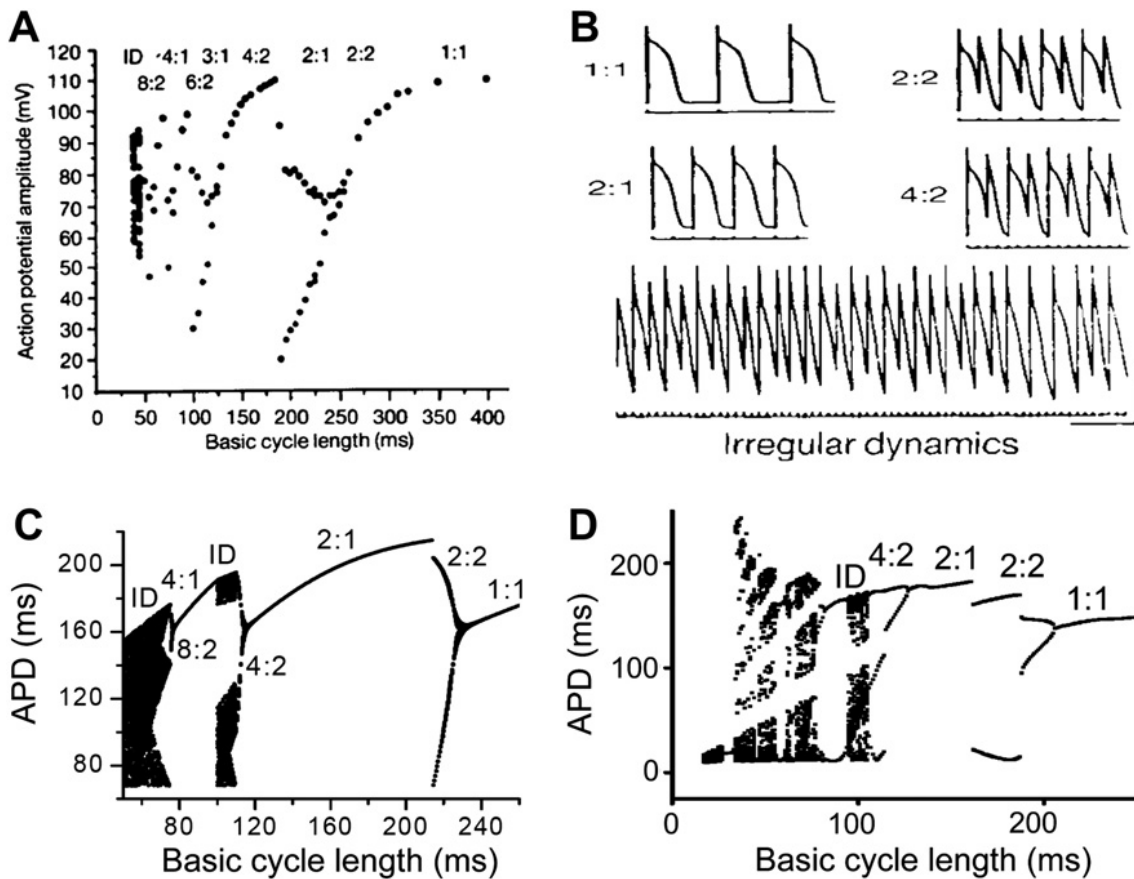


Figure 13. Cardiac chaos. A. Bifurcation diagram showing the relationship between the basic cycle length of pacing and beat-to-beat action potential amplitudes in a sheep cardiac Purkinje fiber. The observed bifurcation sequence is: 1:1/2:2/2:1/4:2/3:1/6:2/4:1/8:2/ID.. "ID" stands for irregular dynamics or dynamical chaos. B. Action potential recordings from a dog cardiac Purkinje fiber at different basic cycle length, showing 1:1, 2:2, 2:1, 4:2, and irregular dynamics. C. Bifurcation diagram showing APD versus basic cycle length from an iterated map. The bifurcation sequence shows: 1:1 / 2:2 / 2:1 / 4:2 / ID / 4:1 / 8:2 / ID. The bifurcation diagram is generated using an exponential APD restitution function. For each CL, the first 40 APDs are discarded and the next 100 APDs are plotted. In the alternans (2:2) regime, there are only two APD values though 100 APDs are plotted, however, in the chaotic regime, the values of the 100 APDs are all different, resulting in scattered plots. D. Bifurcation diagram showing APD versus basic cycle length from a computer simulation using the Beeler Reuter action potential model [16].

In fig. 13 some examples of the chaotic behavior of cardiac tissue are shown. It's important to see that in A there is an experimental bifurcation diagrams and in C and D there are two diagrams, one is obtained in an analytical way using the APD restitution relation (I), (C), the other in a computer simulation (D). These three examples are very similar and show a change in the dynamics of the studied system [16]. The values of CL in which the bifurcations of the diagrams occur are the same values of CL in which alternans occur in APD restitution. So alterans is a manifestation of a change in the dynamics of systems.

2.3 A more complicated APD restitution relation: the memory effect

The APD restitution relation where APD is a function only of the previous DI, given the complexity of the cardiac tissue, is a very simply model and it cannot explain all the faces of the cardiac dynamics; the same is for the criterion suggested by Nolasco and Dahlen: it fails in several experimental situation. These observations suggest that the dynamics of paced cardiac tissue cannot be described by the one dimensional map (III).

2.3.1 Experiments vs theory

Some authors have found that alternans can occur even though the slope of the APD restitution curve is smaller than 1 [17, 19]. Then, another experimental observation is that APD restitution curves depends strongly on the particular pacing protocol used to obtain it. The most used pacing protocols are the following:

- dynamic restitution: the steady-state APD and DI are measured as the basic cycle length (CL) decreases;
- S1-S2 restitution: a premature stimulus (S2) is applied at various times relative to the end of a series of paced (S1) beats and the APD and DI are measured for each S2, fixed S1; then the same thing is made changing the CL_{S1} ;
- constant-BCL restitution: the tissue is paced at a constant CL after a given time, then the CL is shortened and the accommodation of the APD is measured.

Theoretical studies have shown that each of the curves, obtained with these different protocols, captures a different aspect of restitution dynamics: the S1-S2 restitution curve is an indicator of the immediate response to a change in CL, the dynamic restitution curve is a measure of the steady-state response and finally constant-BCL restitution curve is a measure of the transient response linking the previous two. The three restitution curves are different but this fact is in contrast to the predictions of the one dimensional map (IV) [18]. Also the S1-S2 restitution curves exhibit a rate-dependent behavior (it depends on CL_{S1}) which contradicts the one dimensional map (IV).

2.3.2 A new stability criterion

A new model was suggest, on empirical basis, [19] in order to investigate these rate dependent restitutions. The form of the model is the following:

$$APD_{n+1} = F(APD_n, DI_n) \quad (V)$$

In fig. 14 examples of a generic restitution surface F , dynamic restituion (cyan), S1-S2 restitution (red) and constant-BCL restitution (blue) curves and their intersection in a fixed point are shown. From this model a new stability criterion is derived [18].

Alternans occurs if:

$$|F'| = |S_{BCL}| = \left| 1 - \left(1 + \frac{1}{S_{dyn}} \right) S_{S1-S2} \right| < 1 \quad (VI)$$

where S_{BCL} , S_{dyn} and S_{S1-S2} are, respectively, the slopes of constant BCL restitution, dynamic restitution and S1-S2 restitution. According to the criterion (VI) the onset of alternans is determined by a combination of S_{dyn} and S_{S1-S2} and not by either of the slopes individually. The criterion (VI) was applied to a map derived from a cardiac membrane model made by Fenton and Karma [20] and the results of the simulation, shown in fig.15, are pretty good. Such a model is a one dimensional model with memory: in the equation (V) the term APD_n indicates that APD_{n+1} depends, not only on the previous DI, but on the previous APD too. This kind of memory is referred to as short-term memory: it's an intrinsic property of the paced myocardium and reflect the influence of pacing history in a time scale of minutes. Short-term memory is at fault of that restitution relation curves' dependence on pacing protocols which it has been dealt with in the previous paragraph. It was suggested that the Ca_i^{2+} transient plays an important role in the shot-term memory mechanism [21]. Starting from this knowledge, in this work the influence of Ca^{2+} on APD restitution curves and on alternans is studied operating on the $[Ca^{2+}]_e$ like explained in the next chapters. Till now, the Tolkacheva' s criterion is experimentally proofed only in rabbits with satisfying results [22].

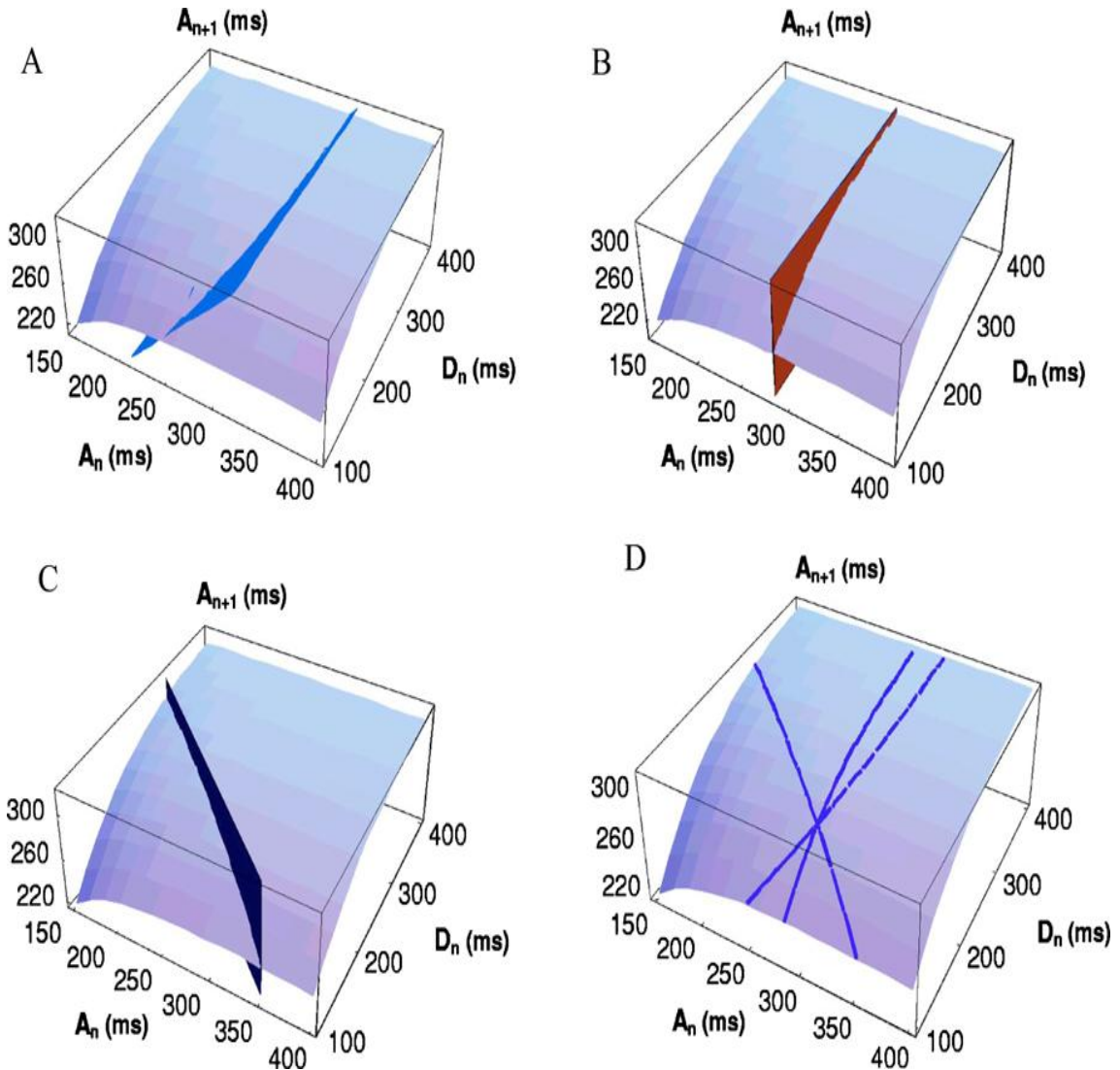


Figure 14. Graphical illustration of (A) dynamic, (B) S1-S2, (C) constant-BCL restitution curves, and (D) their intersection at fixed point of the map (adapted from [19]).

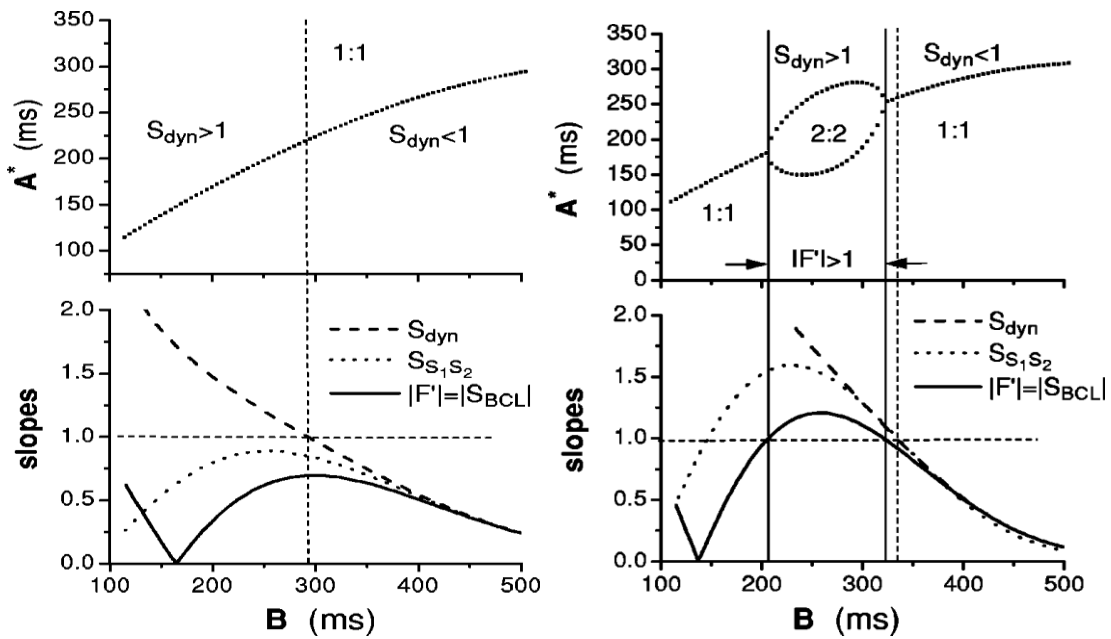


Figure 15. Simulations using the Fenton-Karma model [20]. (Adapted from [19])

2.4 Alternans in cardiac tissue

Although all the past considerations are supported by experimentations and computational modeling, the dynamics of periodically paced whole hearts are more complex, mainly due to the presence of cell-to-cell communication. Therefore, a single restitution curve measured in the heart does not reflect its spatio-temporal dynamics, and thus cannot correctly predict the onset of alternans. Nevertheless, the direct link between the onset of alternans in the heart and local restitution properties is still missing.

2.4.1 Concordant and discordant alternans

In cardiac tissue alternans can be spatially concordant or discordant: spatial concordant alternans (SCA) occur when cells from different regions oscillate in phase, i.e., all cells have long-short sequences of APDs; spatial discordant alternans (SDA) occurs when cells from different special locations oscillate out of phase, i.e., some cells exhibit a long-short sequence while other cells have a short-long sequence (fig. 16). It has been demonstrated [23] that discordant spatial alternans is the primary cause of TWA which is, as written before, a precursor of cardiac lethal arrhythmias.

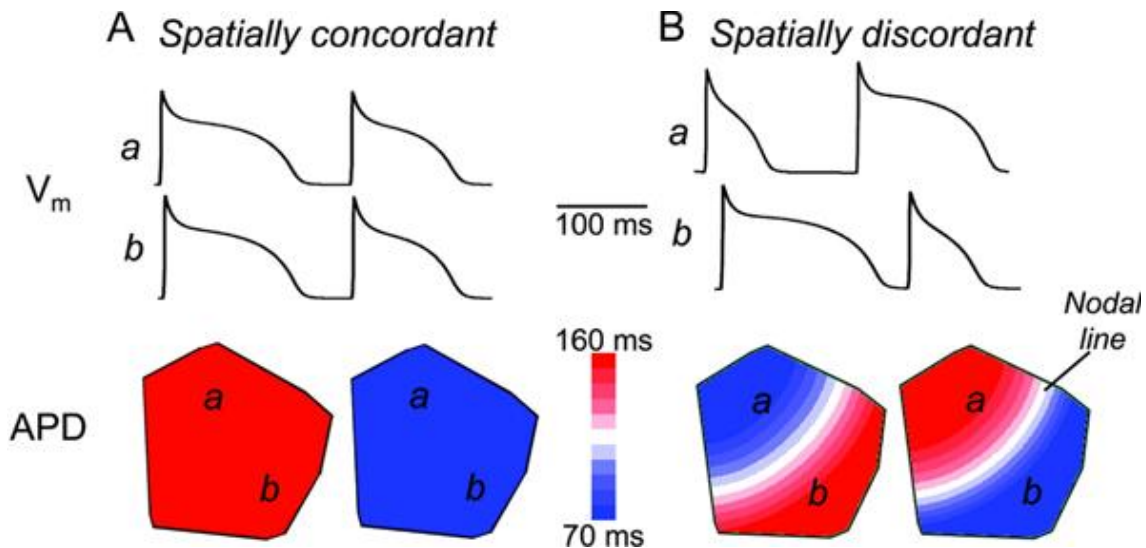


Figure 16. SCA (A) and SDA (B) in simulated 2D cardiac tissue. Top panels: action potentials from sites a and b both alternate in phase in A, and out-of-phase in B. Bottom panels: spatial APD distribution. The nodal line (white) with no APD alternans separates out-of-phase regions (adapted from [24])

Spatially discordant alternans creates a substrate for VF desynchronizing depolarization and increasing dispersion of refractoriness [23, 25-27]. Despite the clearness of arrhythmogenicity of spatial discordant alternans the mechanism underlying its onset is poorly understood. Till now two possible mechanisms have been suggested to explain

the formation of spatial discordant alternans: the first one is related to the presence of heterogeneities in cardiac tissue; the second mechanism is a steep CV restitution curve [3]. Discordant alternans onset and development have been experimentally identified as the most dangerous precursor for the genesis of cardiac fibrillation [28] and related to the induction of reentry in simulated cardiac tissue [29].

2.4.2 Electrical propagating waves

The electric activity of the heart, i.e. the depolarization and the repolarization, propagates in the tissue like a wave. Experimental evidence shows that propagating waves are planar in healthy tissues and are spiral (VT) and break-up spiral (VF) in tissues affected by rhythm disorders. Propagating waves, a manifestation of the dynamics of the heart, are connecting with alternans: some computer simulations showed that when APD alternans occurs also the spiral wave break up occurs [30]. Even though APD alternans is not the unique factor generating the break-up spiral waves surely these waves arise when APD alternans occurs. In fig. 17 the break-up of a spiral wave in presence of alternans in a computational model is shown.

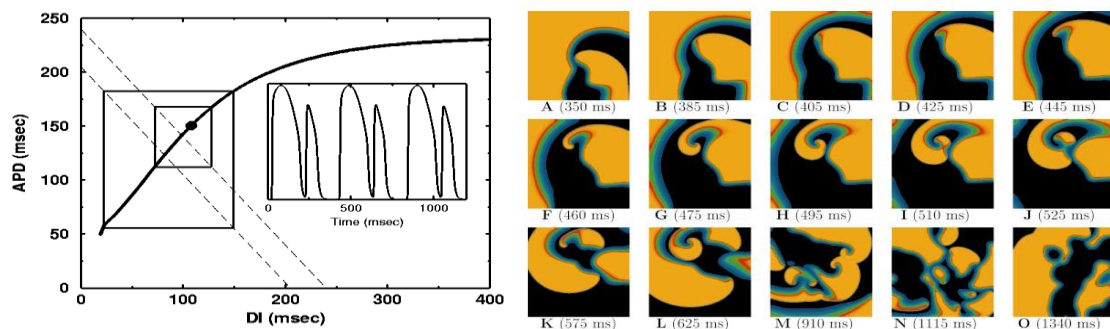


Figure 17. Alternans development and spiral breakup [28]. (LEFT) APD restitution curve with slope greater than one, allowing alternans to develop over a wide range of periods before reaching conduction block. Periods below 260 ms display alternans. (RIGHT) Evolution of breakup close to the tip due to steep APD restitution with wave fronts were blocked by refractory regions resulting in a transient break-up.

2.5 ...to sum up...

Heart can be considered a complex dynamical system with a highly non-linear dynamics, so most of the techniques used to understand its behavior come from the field of dynamical system. APD alternans is one of the most studied phenomenon of the heart's dynamics. This is due to the experimental evidence which consider APD alternans (and the related TWA) a predictor of arrhythmias; so, one of the focal goal in

studying alternans is, starting from the APD restitution curves, to give a criterion which allows to predict the onset of alternans. The first criterion found in literature was suggested by Nolasco and Dahlen but it failed in several cases. This results can be explained referring to the difference between theoretical part and experimental part: e.g. the APD restitution curve from a pure theoretical point of view should be always the same but it actually changes depending on the experimental protocol used in collecting data. A new criterion for the prediction of alternans based on the slopes of different restitution curves has been recently suggested by Tolkacheva and group of the Duke university. Some computer simulations seem to validate this criterion [31] even though there are few experimental results confirming its goodness [22].

BIBLIOGRAPHY

- [1] C.D. Diego, R.K. Pai, A.S. Dave, A. Lynch, M. Thu, F. Chen, L.H. Xie, J.N.Weiss, and M. Valderrábano. Spatially discordant alternans in cardiomyocyte monolayers. *Am. J. Physiol. HeartCirc. Physiol.* 294: 1417–1425, 2008
- [2] M.L. Riccio, M.L. Koller, and R.F. Gilmour. Electrical restitution and spatio-temporal organization during ventricular fibrillation. *Circ. Res.* 84, 955–963, 1999.
- [3] M.A. Watanabe, F. H. Fenton, S.J. Evans, H. M. Hastings, and A. Karma. Mechanisms for discordant alternans. *J. Cardiovasc. Electrophysiol.* 12:196–206, 2001.
- [4] E. Pruvot,, and D. Rosenbaum. T-wave alternans for risk stratification and prevention of sudden cardiac death. *Curr. Cardiol. Rep.* 5, 350–357, 2003
- [5] X. Wan, K. R. Laurita, E. J. Pruvot, and D. S. Rosenbaum,. Molecular correlates of repolarization alternans in cardiac myocytes. *J. Mol. Cell. Cardiol.* 39, 419–428, 2005.
- [6] S. A. Gaeta, and D. J. Christini. Non-linear dynamics of cardiac alternans: subcellular to tissue-level mechanisms of arrhythmia. *Front. Physio.* 3:157 (2012).
- [7] M. R. Guevara, G. Ward, and L. Glass. Electrical alternans and period-doubling bifurcations. *Comput. Cardiol.* 167-170, 1984.
- [8] J. B. Nolasco, and R. W. Dahlen. A graphic method for the study of alternation in cardiac action potentials. *J. Appl. Physiol.* 25, 191–196. 1968.
- [9] [www.scholarpedia.com /restitution](http://www.scholarpedia.com/restitution)
- [10] M. Li, N. F. Otani. Ion channel basis for alternans and memory in cardiac myocytes. *Ann. Biomed. Eng.* 31:1231-1230, 2003.
- [11] J. I. Goldhaberger, X, L. H. Xie, T. Duong, C. Motter, K. Khuu, and J. N. Weiss. Action potential duration restitution and alternans in rabbit ventricular myocytes: the key role of intracellular calcium cycling. *Circ. Res.* 96: 459-466, 2005.
- [12] www.thevirtualheart.org
- [13] S. H. Strogatz. *Nonlinear Dynamics and Chaos: with Applications to Physics, Biology, Chemistry, and Engineering*. Cambridge: Westview Press. 2000
- [14] M.W. Hirsch, S. Smale, R. L. Devaney. *Differential Equations, Dynamical Systems, and an Introduction to Chaos*. 3rd Edition. Academic Press.
- [15] [www.scholarpedia.com /article/Andronov-Hopf_bifurcation](http://www.scholarpedia.com/article/Andronov-Hopf_bifurcation)

- [16] Z. Qu. Chaos in the genesis and maintenance of cardiac arrhythmias. *Progress in Biophysics and Molecular Biology*. 105(3): 247-257, 2011.
- [17] R. F. Gilmour, N. F. Otani, and M. A. Watanabe. Memory and complex dynamics in cardiac Purkinje fibers. *Am. J. Physiol.* 272: H1826-H1832, (1997)
- [18] E. G. Tolkacheva, D. G. Schaeffer, D. J. Gauthier, W. Krassowska. Condition for alternans and stability of the 1:1 response pattern in a “memory” model of paced cardiac dynamics. *Phys. Rev. E*. 67:031904 (2003).
- [19] N. F. Otani, and R. F. Gilmour. Memory models for electrical properties of local cardiac systems. *J. Theor. Biol.* 187: 409-436, 1997.
- [20] F. H. Fenton, and A. Karma. Vortex dynamics in three-dimensional continuous myocardium with fiber rotation: filament instability and fibrillation. *Chaos*. 8:S1054-S1500 (1998).
- [21] H. Zang, T. Ueyama, J. Wang, R.J. Wu, and S.F. Lin. Short-term and electrical restitution in the canine transmural ventricle. *Physiol. Meas.* 32:207-222 (2011).
- [22] S. S. Kalb, H. M. Dobrovolny, E. G. Tolkacheva, S. F. Idriss, W. Krassowska, and D. Gauthier. The restitution portrait: A new method for investigating rate –dependent restitution. *J. Cardiovasc. Electrophysiol.* 15: 698-709 (2004).
- [23] J. M. Pastore, S. D. Girouard, K. R. Laurita, F. G. Akar, and D. S. Rosenbaum. Mechanism linking t-wave alternans to the genesis of cardiac fibrillation. *Circulation* 99, 1385-1394 (1999).
- [24] J. N. Weiss, A. Karma, Y. Shiferaw, P. S. Chen, A. Garfinkel, Z. Qu. From pulsus to pulseless: the saga of cardiac alternans. *Circ. Res.* 98: 1244–1253 (2006).
- [25] Konta, T., Ikeda, K., Yamaki, M., Nakamura, K., Honma, K., Kubota, I., Yasui, S.: Significance of discordant ST alternans in ventricular fibrillation. *Circulation* 82: 2185– 2189 (1990).
- [26] Rubenstein, D.S., Lipsius, S.L.: Premature beats elicit a phase reversal of mechanoelectrical alternans in cat ventricular myocytes: a possible mechanism for reentrant arrhythmia. *Circulation* 91: 201–214 (1995).
- [27] H. Tachibana, I. Kubota, M. Yamaki, T. Watanabe, H. Tomoike. Discordant S-T alternans contributes to formation of reentry: a possible mechanism of reperfusion arrhythmia. *Am. J. Physiol.* 275: H116–H121 (1998).
- [28] J. M. Pastore, S. D. Girouard, K. R. Laurita, F. G. Akar, and D. S. Rosenbaum. Mechanism linking T-wave alternans to the genesis of cardiac fibrillation. *Circ.* 99:1385–1394, (1999).
- [29] Z. Qu, A. Garfinkel, P. S. Chen, and J. N. Weiss. Mechanisms of discordant alternans and induction of reentry in simulated cardiac tissue. *Circ.* 102:1664-1670 (2000).

- [30] F. H. Fenton, and E. M. Cherry. Multiple mechanisms of spiral wave breakup in a model of cardiac electrical activity. *Chaos*, 12:852-892, (2002).
- [31] E. Cherry, F. H. Fenton. of alternans and conduction blocks despite steep APD restitution: electrotonic, memory, and conduction velocity restitution effects. *Am J Physiol Heart Circ Physiol* 286: H2332–H2341 (2004).
- [22] S. S. Kalb, H. M. Dobrovolny, E. G. Tolkacheva, S. F. Idriss, W. Krassowska, and D. Gauthier. The restitution portrait: A new method for investigating rate-dependent restitution. *J. Cardiovasc. Electrophysiol.* 15: 698-709 (2004).

3. The experimental protocol

This chapter deals with the experimental part of this work. The optical mapping is introduced as a technique used to collect simultaneous AP recordings from the endocardium and the epicardium; then a custom made Java code, developed by Dr. Alessio Gizzi and Prof. Flavio H. Fenton, was used to analyze the collected data.

3.1 Data acquisition: the optical mapping technique

Membrane potential has generally been studied by intracellular recordings from cells impaled with glass pipette microelectrodes, but in 1968 a new technique, the optical mapping technique was first used [1] and ten years later optical APs were recorded from mammalian hearts by using voltage-sensitive dyes [2]. Nowadays the optical mapping of the heart is a very common lab technique. The optical mapping method is very useful and allows simultaneously recordings of membrane potential from multiple sites (typically thousands). The goal of the optical mapping system is to provide optical signals with a high SNR and high temporal and spatial resolution, while minimizing the probability of side effects, including photobleaching. All cardiac optical mapping acquisitions require staining the heart with voltage-sensitive and/or calcium dye and then using imaging systems to record electrical activity and calcium transients from the surface of the heart.

3.1.1 Voltage-sensitive dyes and detectors

Voltage-sensitive dyes contain molecules that selectively bind to cell membranes when cardiac tissue is perfused or superfused with them [3; 4]. How do voltage-sensitive dyes work and why are they important? Very simply it can be said that the dye molecules fluorescence light in direct proportion to trans-membrane voltage: when the membrane voltage changes also the fluorescence intensity changes. For any given constant excitation light intensity and wavelength, light is emitted over a range of wavelengths (emission spectra) that changes with membrane potential (fig. 17). Optical measurements are indicated either as a change in fluorescence (ΔF) or as a fractional fluorescence change ($\Delta F/F$ is the change in fluorescence intensity during a given voltage step divided by the background fluorescence; [5]). The $\Delta F/F$ corresponds to

depolarization during an AP recording (approximately 100 mV). It's important to notice that $\Delta F/F$ does not reflect the absolute resting membrane potential because of some side effects such as tissue auto-fluorescence, bleaching, or the loss of the dye from the tissue. There are two great families of voltage-sensitive dyes: fast response dyes and slow response dye. Only fast voltage-sensitive dyes are used in cardiac electrophysiology because of their response that occurs in the temporal scale of microseconds; thus, APs can be measured. Although optical recordings reproduce the temporal course of APs, they do not provide absolute values of membrane potential voltages [3-4].

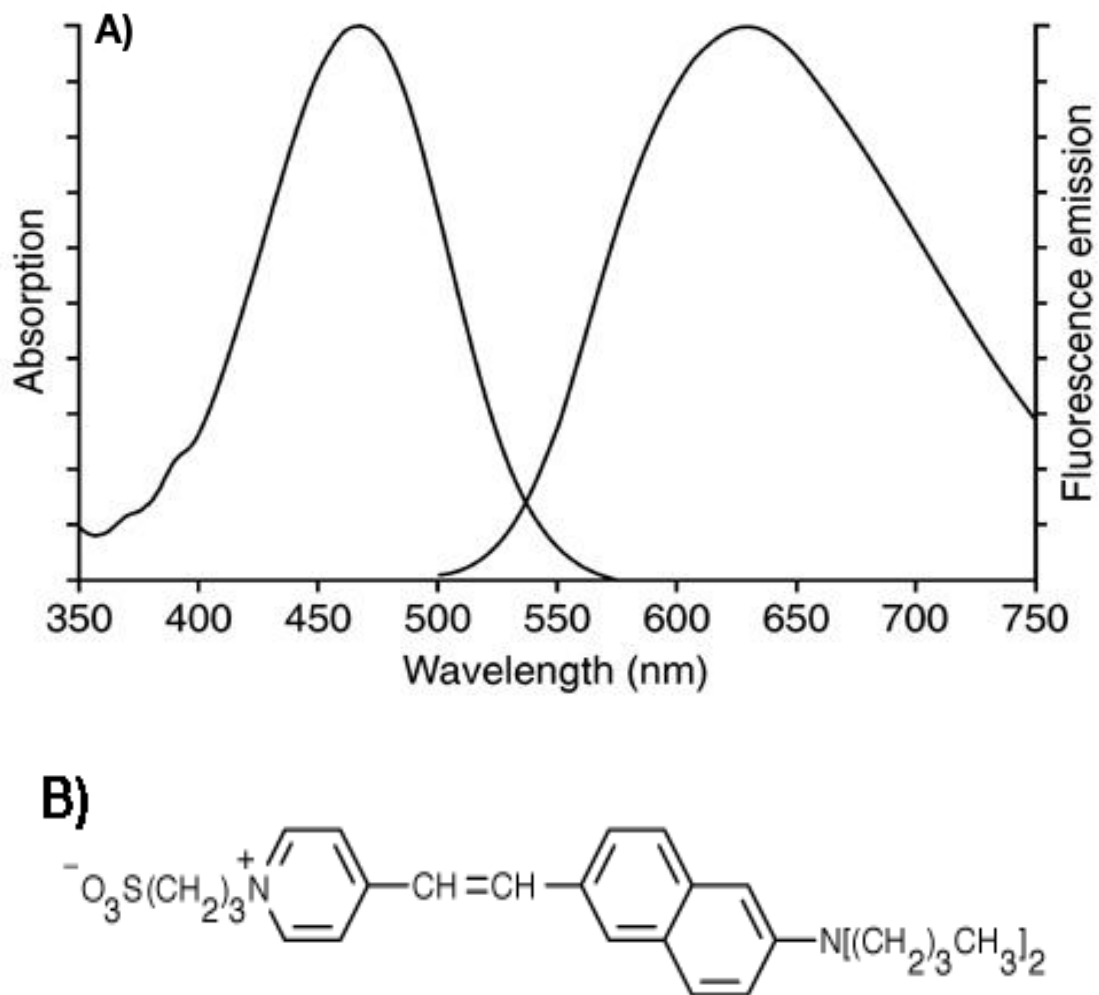


Figure 17. (A) The absorption and emission spectra of a dye and (B) the chemical structure of Di-4-ANEPPS, one of the most popular and used voltage-sensitive dye in cardiac electrophysiology (adapted from [6]).

The changes in the emitted light is captured by some detectors with particular light-sensitive filters. This detectors, or photodetectors, can be both photodiode arrays and charged coupled device (CCD) video cameras. A photodiode is a semiconductor junction that converts light into current. The current needs to be amplified and the must be passed to a current-voltage converter and, finally, is sent to a data acquisition computer. Such an array can contain several hundred photodiodes and they have a high sampling rate. The CCD video camera is a semiconductor device segmented into several pixels, permitting a greater spatial resolution between recording sites: photo-excited charge carriers are collected within a single pixel over a finite period of time (integration time), and are read off at regular time intervals (i.e. the frame rate). Readout time is a major factor that limits the sampling rate of CCD systems. Figure 18 shows an optical stup.

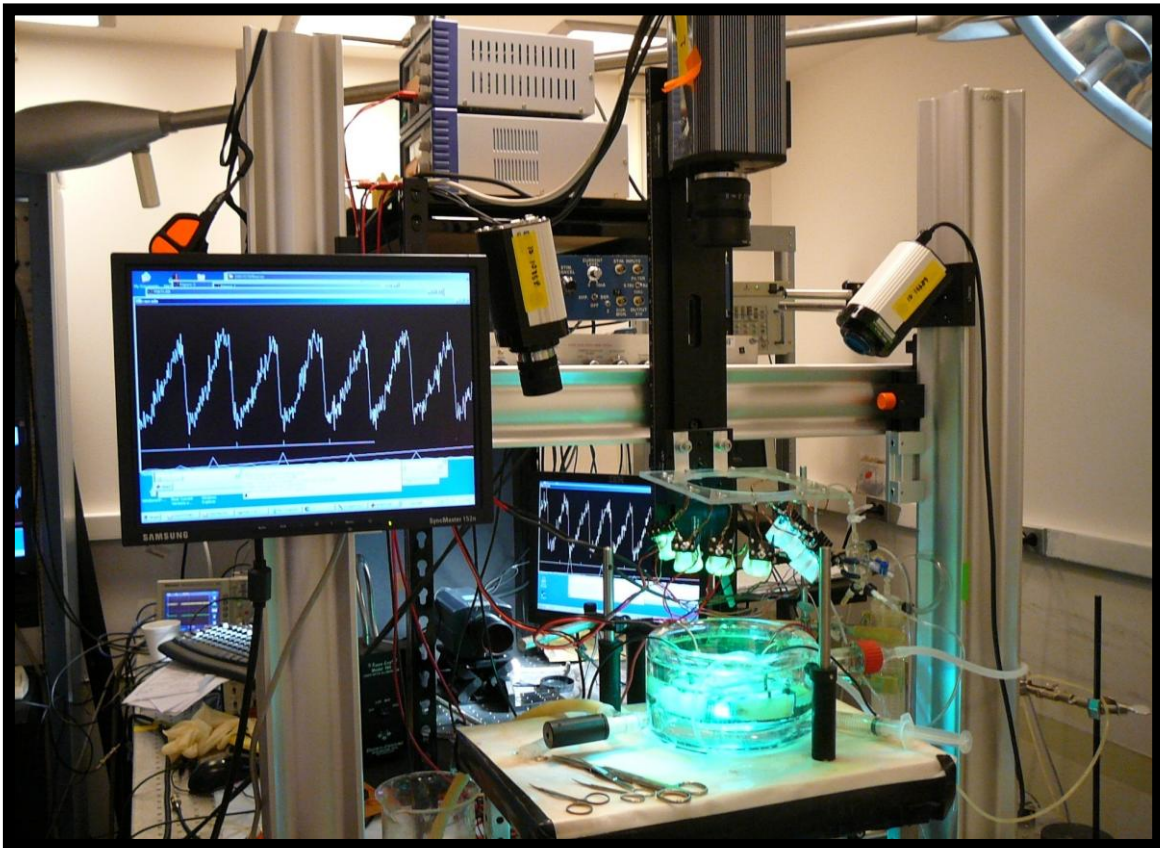


Figure 28. Optical mapping room. Gilmuor Lab, College of Veterinary Medicine, Cornell University, Ithaca, NY, USA. The picture shows the optical mapping setup. Cameras, used to record data, are visible; in the screen areal time AP acquisition is shown.

3.2 Data collecting: the preparation of cardiac tissue

In order to answer the questions about the behavior of cardiac tissue in low calcium conditions 5 beagles (dogs) (n=5) of either sex, 1-4 years old, were anesthetized (put down) with Fatal-Plus (390 mg/ml pentobarbital sodium; 86 mg/kg iv; Vortech Pharmaceutical, Dearborn, MI), and their hearts were explanted rapidly and placed in cool and oxygenated (95% O₂-5% CO₂) canine Tyrode solution. Quickly the right ventricle (RV) was excised, the right coronary artery was cannulated and then the tissue was clamped in order to ensure an optimal perfusion (fig. 19).



Figure 19. A good example of tissue preparation. (Left) Canine right ventricle, endocardium: it is possible to see the clamps and the cannula perfusing the right coronary artery. (Right) Canine left ventricle, epicardium (courtesy of Prof. Fenton) .

The right ventricle (RV) was placed into a heated transparent water jacketed custom made glass container and perfused with a peristaltic pump, pumping the canine Tyrode solution at a constant flow rate of 25ml/min into the right coronary artery via a bubble trap. This trap allows to stop bubbles before penetrating into the tissue causing embolisms.

Normal canine Tyrode Solution	
COMPONENTS	QUANTITY [mM]
MgCl ₂	0.5
NaH ₂ PO ₄	0.9
CaCl ₂	2.0
NaCl	137
NaHCO ₃	24
KCl	4.0
Glucose	5.5

Tab.1. Canine Tyrode solution with concentrations of components.

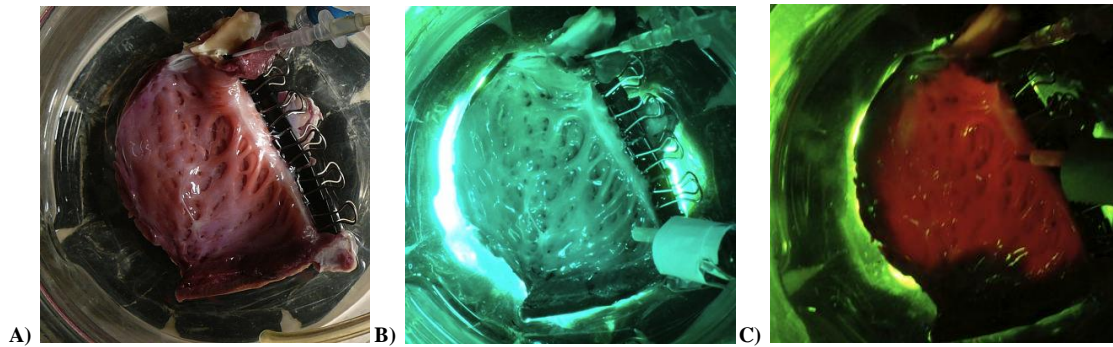


Figure 30. Tissue illumination and emission: (A) natural light view; (B) illuminated tissue at 530nm; (C) infrared tissue light emission (Courtesy of Prof. Fenton).

After 20 to 30 minutes of equilibration at physiological temperature ($37.0 \pm 0.5 \text{ }^\circ\text{C}$), the voltage-sensitive dye Di-4-ANEPPS ($\mu\text{10 mol/l bolus}$) was used in order to stain the preparation. In fig.20 is shown the effect of the Di-4-ANEPPS on the tissue. This dye was chosen because of its fast response to a voltage change, optimal for capturing the transient potential changes. Moreover Di-4ANEPPS is quickly absorbed by tissue ($\sim 15\text{-}20 \text{ min}$). Blebbistatin ($10 \text{ }\mu\text{mol/l}$ constant infusion over 30 to 40 minutes) was added to prevent motion artifact [7]. Finally a Tyrode solution with a low calcium concentration (hypocalcemia) (0.0625mM) was used. Three experiments of five were performed only in low calcium conditions. All experimental procedures were approved by the Institutional Animal Care and Use Committee of the Center for Animal Resources and Education at Cornell University.

3.2.1 The optical setup

The optical setup could be divided schematically into four blocks:

- The “heart” of the optical setup is the water-jacketed chamber where the cannulated tissue is contained;
- The perfusion system and the bath, connected to an heater in order to have an accurate control over the temperature.
- The illumination system, placed both on top and bottom of the tissue;
- The CCD cameras recording synchronously endocardial (top) and epicardial (bottom) surfaces. The bottom camera is not directed towards the epicardial surface but a mirror is positioned below the tissue chamber and reflects the image of the tissue towards the camera.

In fig. 21 a flowchart shows the main components of the optical setup.

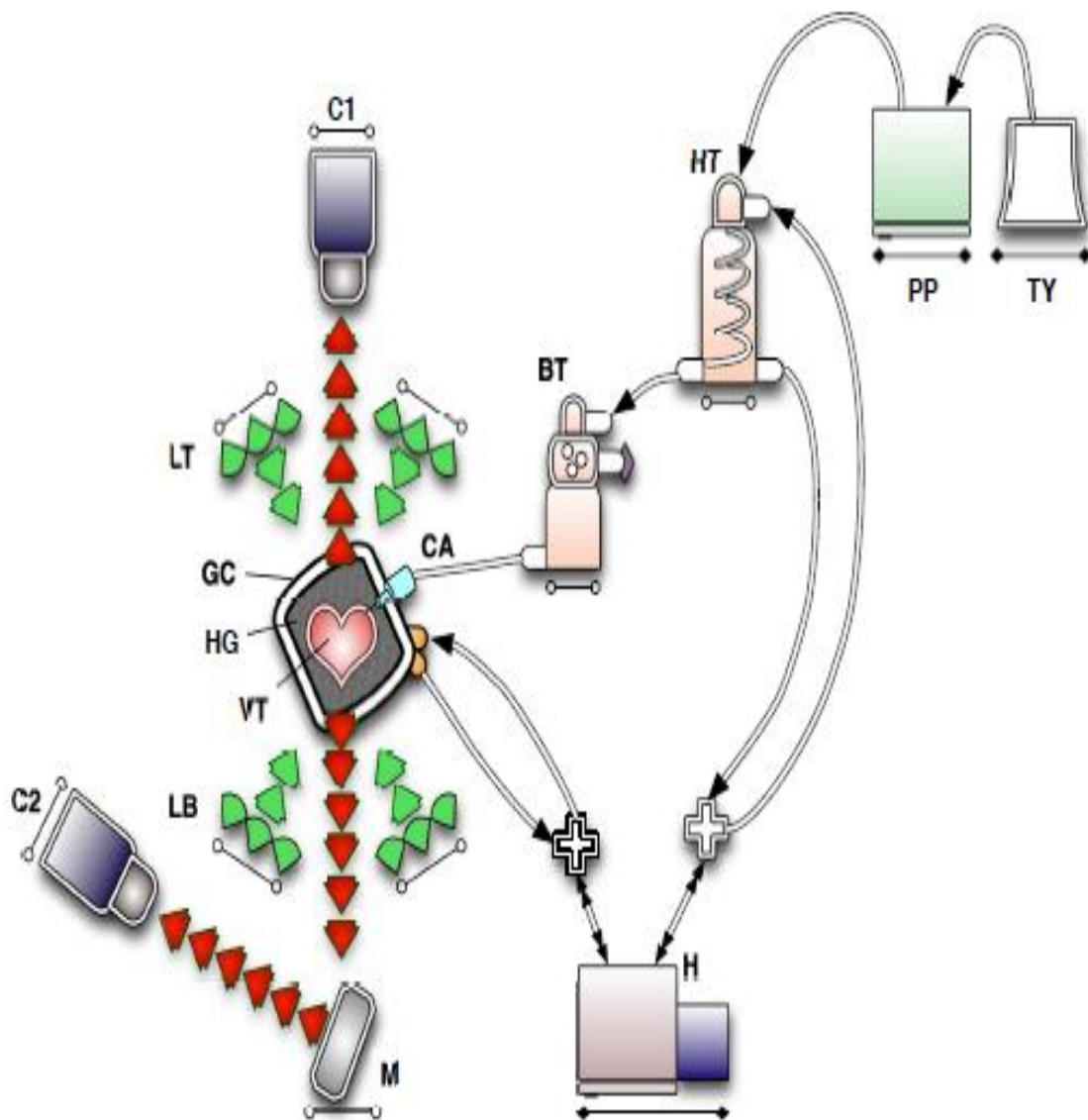


Figure 21. Flowchart of the optical mapping setup designed for alternans recordings. The main components are reported and specifically labeled. Ventricular tissue, VT; right coronary artery with a plexiglas syringe cannulation, CA; the specimen is fixed through an holding grid, HG, and contained into a glass chamber, GC. Selective light lamps from the top, LT, and the bottom, LB. The light emitted from the tissue is directly captured by a top camera, C1, for the endocardial surface, and via a directional mirror, M, by a bottom camera, C2, for the epicardial surface. Both cameras are equipped with an emission filter EF1, EF2. The peristaltic perfusion pump, PP, supplies the tissue with oxygenated tyrode solution, TY, which is continuously dribbled in a bubble trap, BT, in order to avoid the presence of any dangerous gas bubbles which could The heat bath, H, used for accurate temperature control (adapted from [6]).

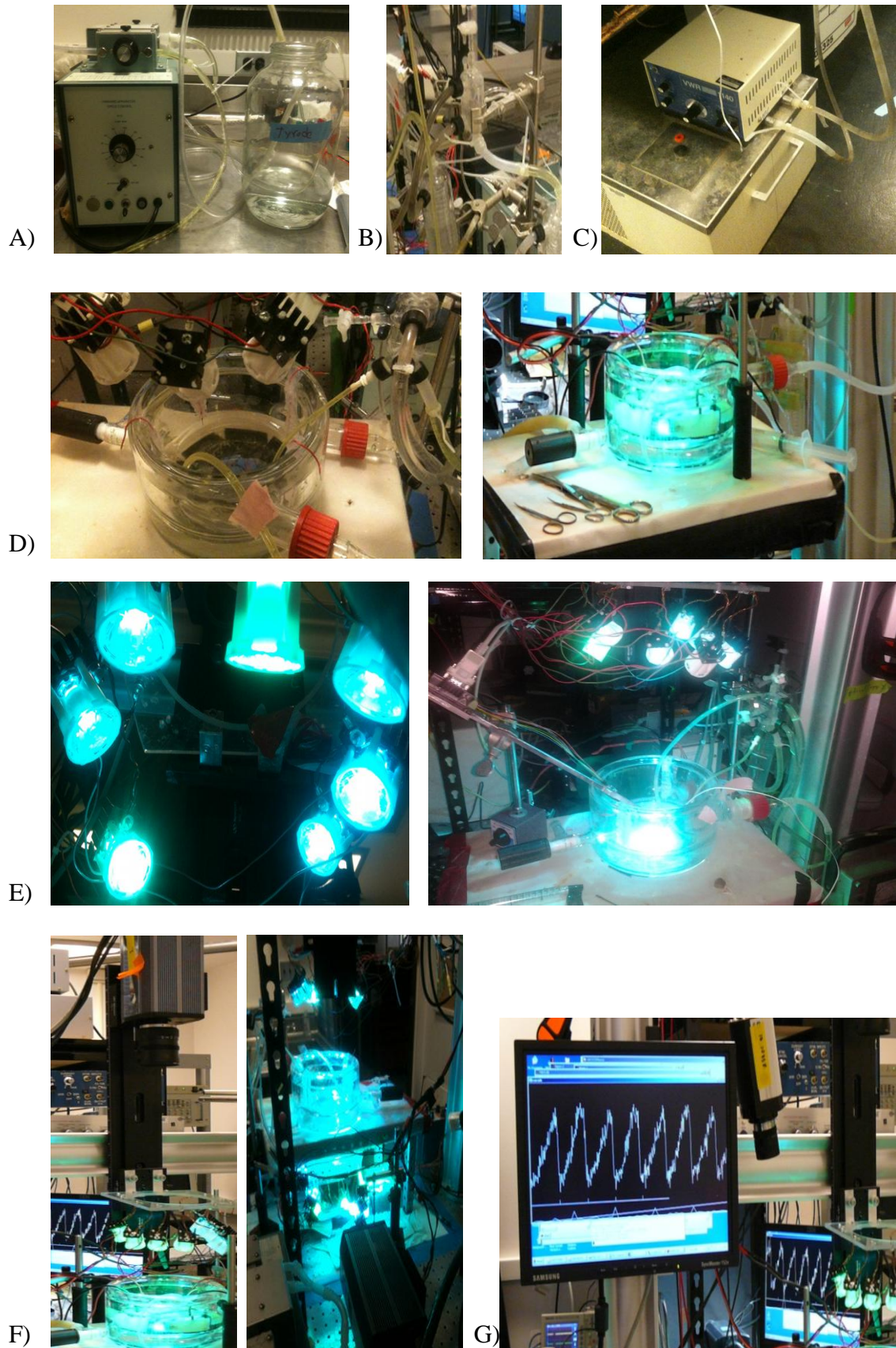


Figure 22. The main components of the optical set up: the perfusion system and its parts: (A) the peristaltic pump; (B) the bubble trap; (C) the heater; (D) the water-jacketed glass chamber from different views; the illumination system: (E) the green led; (F) The top CCD video camera pointing to the chamber and the CCD bottom video camera pointing to the mirror under the glass chamber; (G) the two monitors displaying the real-time signals.

The perfusion system, shown in fig.22(A-D), is made up of a peristaltic pump, pumping the Tyrode solution at constant flow rate in the tissue via a system of transparent silicon tubes terminating in a heating coil and a bubble trap. This allows a continuous control of the delivered solution avoiding the presence of air bubbles, which would lead to embolisms of the tissue. A heater is connected both to the coil and the water-jacketed chamber in order to make a closed circulatory system, which allows the accurate temperature control of both the tissue and the perfusate. The illumination system is shown in fig.22(E). Excitation light consists of high-performance light-emitting diodes (Luxeon III star, LXHL-FM3C, wavelength 530 nm), eight for the top view and eight for the bottom view, driven by a low-noise constant-current source. Collimator lenses (Luxeon, LXHL-NX05) improved the illumination efficiency. To get a simultaneous imaging of the epicardium and the endocardium imaged two synchronized cameras were used (the top and bottom camera are shown in fig.22(F)). The fluorescence emission light was collected for each camera by a Navitar lens (DO-2595, focal length 25 mm, F# 0.95), passed through a long-pass filter ($< 610\text{nm}$), and imaged by a 128×128 back-illuminated electron-multiplied CCD array (Photometrics Cascade 128+) with a high quantum efficiency (peak QE $> 90\%$). The signal was digitized with a 16-bit analog/digital converter at a frame rate of 511Hz (full frame, 128×128 pixels) with a spatial resolution of $600 \mu\text{m}$ per pixel for a grid size of $7.7 \text{ cm} \times 7.7 \text{ cm}$. The peripheral component interconnect interface provided high-bandwidth uninterrupted data transfer to the host computer. Two monitors allowed to follow real time signal from both cameras (fig. 22(G)).

3.2.2 Stimulation protocols

Platinum stimulating electrode connected with a programmable stimulator (Bloom DTU 215B, Bloom Electrophysiology) has been used to pace the right ventricles from the endocardial surface. Data were recorded in episodes lasting between $5\div 10$ s. Two different temporal pacing protocols were applied:

1. Pacing-down protocol (Dynamic pacing protocol). Twice diastolic threshold current pulses were applied with the pacing cycle length (CL) starting from 600 ms and decreasing of 50 ms until reaching 250 ms after which the CL was shortened in 10 ms increments until VF was induced or 2:1 block occurred. For each CL the signal was recorded after $10\div 15$ s in order to get ADP and DI at the steady state.

2. Dynamic-S1-S2 Protocol. Twice diastolic threshold current pulses were applied pacing the tissue at a constant CL starting from 900 ms and decreasing by 100 ms till a CL of 600 ms was reached, and then decreasing by $50 \div 10$ ms till VF was induced or 2:1 block occurred. These main CLs could be called S1. From 600 ms on, before decreasing the CL 51 beats were delivered: 50 at the same CL while the last one (S2) with different CLs. The stimulus S2 was progressively shortened and APD and DI were measured for every S2.

In order to prevent the premature onset of VF, for the fastest S1 the stimuli S2 were smaller than the S1. The pacing electrode was fixed at the same anatomical position on the endocardium, in all the 6 preparations. The chosen place is the base of the RV in order to re create a sort of pathway of the physiological electrical stimulation. More than 100 recordings were made up for each preparation and considering the number of the pixels of the CCD cameras, thousands of AP were obtained from each recording.

3.3 Data analysis: the Java code

Once obtained, data were analyzed using a specific toolbox developed by Prof. F. H. Fenton and Dr. A. Gizzi [6, 8], allowing the treatment of such a great number of data. A screenshot of the running software interface is shown in fig. 23. The most interesting characters of this software can be found in its extreme flexibility (visualized as shaded arrows in the scheme) and visualization tools:

- the possibility of loading different kinds of file types and video dimensions, i.e. there is no restriction about the space and time scales and durations;
- the possibility to perform different operations several times, such as “time-average”, “space-average” or “signal drifting” tuning the algorithm parameters, i.e. Gaussian variance, shifting frequency, etc.;
- the calculation of many different signal properties, as well as to save movies, images, phase patterns and APD-DI distribution at any time of the analysis;
- it does not impose any fixed sequence of actions, allowing a tunable and personal analysis methodology depending on the data type;
- finally, its visualization tools allow to compare the signal analysis at different steps (thus maintaining in memory all the necessary information):

- stop/resume forward/resume backward movies or APD spatial distribution sequences;
- visualize APD-DI restitution distribution, mean values (also in case of alternating signals) and error bars;
- zooming in and out on both the signal and the distributions;
- plotting the single pixel time evolution during a movie and selecting in real time different kind of pixel or signals;

3.3.1 Methods of analysis: filtering and removing signal drift.

Starting from an initial display settings, the operator can choose which kind of data to study. If the signal has not been analyzed before, four automatic processes are performed. In particular è [6]:

1. the data type is converted in short format, described by 16 Bit and ranging over $-32.768 \div 32.767$, thus obtaining the “original” signal on which the analysis is applied;
2. the casual saturation of the camera, due to the limited number of dedicated bytes is corrected recovering the right time sequence, thus “unwrapping” the signal as:

```

i f ( ( i n t ) ( M a t h . a b s ( m a x [ i ] [ j ] - m i n [ i ] [ j ] ) ) > 30000 ) {
    f o r ( i n t k = 1 0 ; k < ( n t i m e s - 1 0 ) ; k + + ) {
        u [ i ] [ j ] [ k ] = ( s h o r t ) ( u [ i ] [ j ] [ k ] - 2 0 0 0 0 );
        u n w r a p p e d [ i ] [ j ] [ k ] = u [ i ] [ j ] [ k ];
    }
}

```

where “max” and “min” represent the maximum and minimum values of the signal in a given pixel, “u” is the matrix of the original signal and “unwrapped” the resulting unwrapped one. As it can be noted, if the saturation condition holds, the signal is subtracted of a fixed amount of 20.000 in order to recover the right sequence;

3. the unwrapped signal is averaged in time on a 7 pixel basis (3 forward and 3 backward);

4. the signal is conveniently normalized on a pixel-by-pixel basis in the range 0÷10.000. This choice is suitable for subsequent calculation purposes, but it is important to note that the chosen normalization range does not affect the result, being a simple rescaling of the data.

After these four automatic steps the operator can manually improve the signal in the following way:

- the operator interactively defines the so called “mask”, i.e. the area imaged by the camera not part of the tissue, in order to avoid not useful and misleading calculations. In fact, any subsequent analysis is not performed for the selected pixels;
- the analysis continues with a symmetric weighted Gaussian space average. In particular the operator can choose the weighting coefficient, w^2 , in the range 4÷8, representing the variance over the neighbor pixels:

$$G(x, y) = A \exp \left[\frac{-((x - x_0)^2 + (y - y_0)^2)}{-2w^2} \right]$$

and $A= 9000$ has been held fixed.

- An important and well known problem in analyzing optical mapping data consists in removing the signal drift (see Fig.(5.3.4)). In the present code, a dedicate algorithm has been developed to perform such a task.
- Finally, the operator interactively defines the time interval (indicated as ROI, region of interest) over which evaluates all the interesting signal properties.
- As represented by the shaded arrows in Fig.(5.3.2), any of the analysis step can be repeated several times or exchanged in the most suitable order which can lead to the best signal analysis.

Now the main properties of the signal can be extracted, visualized and saved. APD and DI can be automatically evaluated by choosing the appropriate threshold: a common choice is usually to take a threshold in the range 25÷30% of the depolarization; in these experiments the APD and DI are calculated at 25% of depolarization. This variability depends on several factors related to the optical measurement (gain, illumination, frames, etc.), but also on the pacing cycle length. In fact, at high pacing frequencies, tissue repolarization can not be fully recovered, thus requiring a small increase in the threshold value. Usually a value of 25% is a good compromise. This and several others

not unexpected effects (i.e. motion artifacts), make the optical mapping analysis not fully automatable, requiring a careful inspection by the operator.

3.3.2 Alternans phase definition.

To determine the temporal distribution of APD alternans across the mapped field, the difference between two consecutive APDs was computed as:

$$\Delta APD(x, y)_n = APD(x, y)_{n+1} - APD(x, y)_n = \begin{cases} |\Delta APD(x, y)_n| > 2 \text{ ms} & \text{Alternans (RED - BLUE)} \\ |\Delta APD(x, y)_n| \leq 2 \text{ ms} & \text{Nodal line (WHITE)} \end{cases}$$

where n denotes the beat number, and APD(x,y) is the duration of the action potential for a pixel in position (x,y) in the 2D mapped field. Due to our temporal resolution, 2ms, tissue has been defined as alternating when $\Delta APD(x,y)_n$ was smaller than -2 or greater than 2 ms, and as non-alternating otherwise. Such a choice, considering a time interval double of the frame rate (4 ms), induces an accurate distinction between alternating and non-alternating regions. Nevertheless, an interpolating procedure is further performed in order to select the correct threshold timing, thus leading to an even more robust and accurate definition [6].

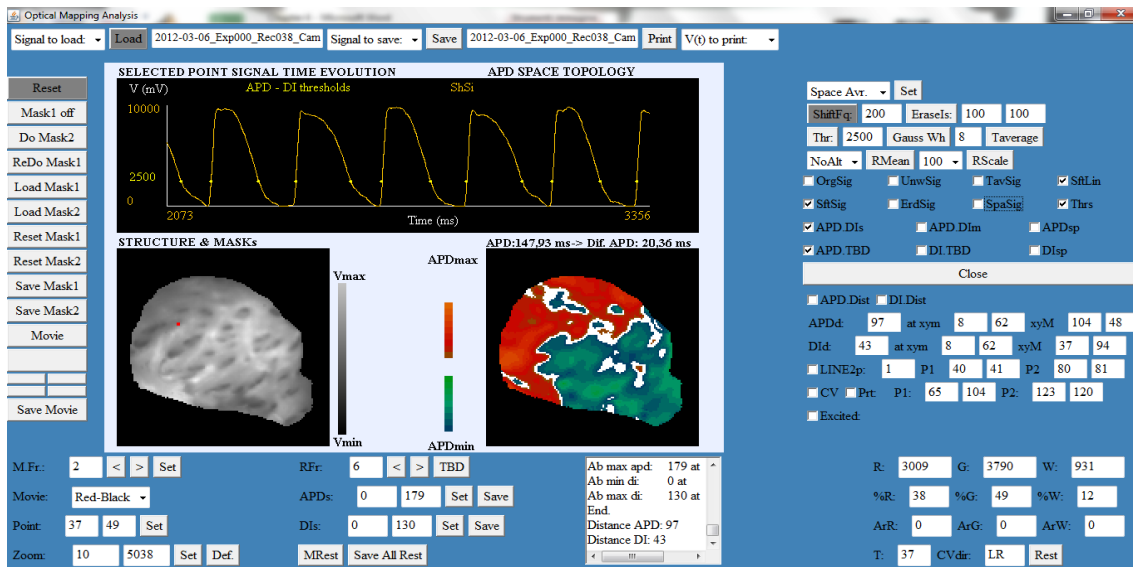


Figure 23. A screenshot showing the Java code running on a pc HP Microsoft Windows 7. It is possible seeing the AP signal (yellow) displaying alternans on the top; the tissue structure on the left and the spatial distribution of alternans on the right. Red means a long-short APD sequence while blue means a short-long APD sequence. Between red and blue there is a white zone representing the nodal line. On the top-right there are the commands for operating on the signal and on the left the buttons for doing, saving and loading masks.

This methodology has been previously adopted by Fenton and Karma [9]. An example of the analysis made with the Java code is shown in fig. 23. The phase of alternans was

defined negative for short-long APD sequences (blue scale) and positive for long-short APD sequences (red scale). Nodal lines were defined as areas separating out-of-phase regions of discordant alternans in which the amplitude of alternans was below the described threshold. Two-dimensional alternans maps were constructed to explore the spatial distribution of the amplitude and phase of the alternans. The onset of alternans (both concordant, CA, or discordant, DA) in tissue was defined separately between endocardial and epicardial surfaces, as the CL at which at least 5% of the surface pixels displayed APD alternans greater than 2 ms. The local CV was only measured in the direction of the propagation wave through the distributions of activation times for spatial regions of 7×7 or 8×8 pixels and fitted with the plane.

3.3.3 Restitution curves

As final step, in order to plot the restitution curves and the bifurcation diagrams four points in the endocardium and four in the epicardium were chosen, as shown in fig. 24 (there wasn't a precise criterion in choosing points but having points in different parts of the tissue); for each point the APD and DI values were obtained from the Java code and the plotting was made with Microsoft Excel.

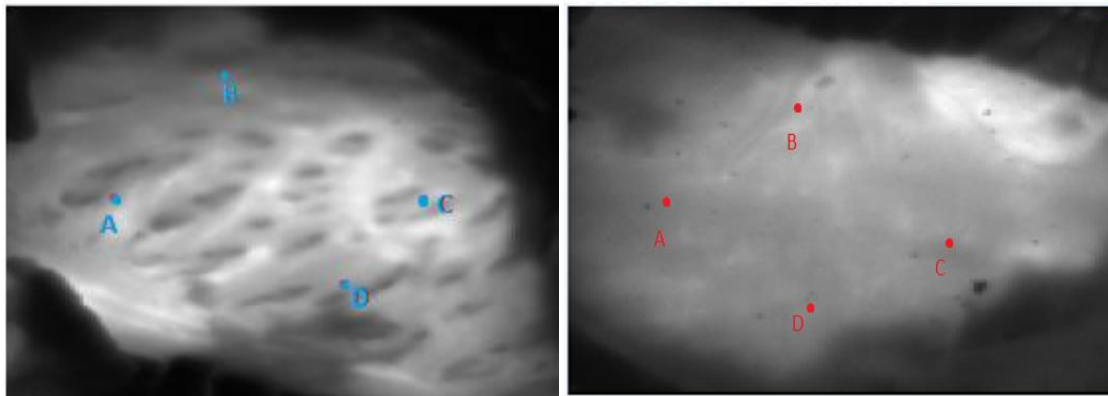


Figure 24. The chosen points in the endocardium (LEFT) and in epicardium (RIGHT).

BIBLIOGRAPHY

- [1] L. B. Cohen, R. D. Keynes, B. Hille. Light scattering and birefringence changes during nerve activity. *Nature*. 218:438-441.(1968)
- [2] G. Salama and M. Morad. Merocyanine 540 as an optical probe of transmembrane electrical activity in the heart. *Science*, 191, 485-487.(1976)
- [3]J. W. Lichtman and J. A. Conchello. Fluorescence microscopy. *Nature Methods*, 2, 910-919 (2005)
- [4]D. S. Rosenbaum . Optical mapping of cardiac excitation and arrhythmias: A primer. In D. S. Rosenbaum, & J. Jalife (Eds.), *Optical mapping of cardiac excitation and arrhythmias* (pp. 2-7). *New York: Futura Publishing*. (2001)
- [5] S. Rohr. Optical mapping of microscopic impulse propagation. In C. Cabo, & D. S. Rosenbaum (Eds.), *Quantitative cardiac electrophysiology* (pp. 507-554).New York: Marcel Dekker (2002)
- [6] A. Gizzi. *Spatio-Temporal Dynamics of Cardiac Physiopathology. Experiments, Theory and Simulations* (2012).
- [7] V. V. Fedorov, I. T. Lozinsky, E. A. Sosunov, E. P. Anyukhovskiy, M. R. Rosen, C. W. Balke, and I. R. Efimov. Application of blebbistatin as an excitation-contraction uncoupler for electrophysiologic study of rat and rabbit hearts. *Heart Rhythm*. 4:619-626. (2007)
- [8] A. Gizzi, E. Cherry, R. F. Gilmour, S. Luther, S. Filippi and F. H. Fenton. Effects of pacing site and stimulation history on alternans dynamics and the development of complex spatiotemporal patterns in cardiac tissue. In press.
- [9] F. H. Fenton and A. Karma. Vortex dynamics in three-dimensional continuous myocardium with fiber rotation: filament instability and fibrillation. *Chaos*. 8:S1054-S1500 (1998).

4. Results and Discussion

In the following the results of this work will be presented at the light of the present knowledge introduced in chapter 3. The suite Microsoft Excel was used in order to post process data. In order to have the best fitting of the experimental points (the restitution curves) and calculate the first derivatives with respect to the DI, and hence the slope of the curves, the root mean square method was used with an exponential function of the form

$$APD = \alpha + \beta e^{-DI/\tau} \quad (1)$$

Finally, conclusions, limitations and future developments will be briefly discussed.

4.1 Results

The main results of this work will be summed up as follows:

1. *the effects of hypocalcemia on VF;*
2. *the effects of hypocalcemia on the slopes of the dynamic restitution curves and on alternans;*
3. *the effect of hypocalcemia on short-term memory;*
4. *the effect of hypocalcemia assessed with the Tolkacheva' criterion.*

To have a better comprehension of the results it's necessary to explain each of them.

4.1.1 The effects of hypocalcemia on VF

VF was induced in every (n=5) experiments in low calcium (LC) condition (hypocalcemia) and in 1 (over 2) experiment with normal Tyrode's solution (NT). In fig. 25 two examples of VF in LC condition are shown.

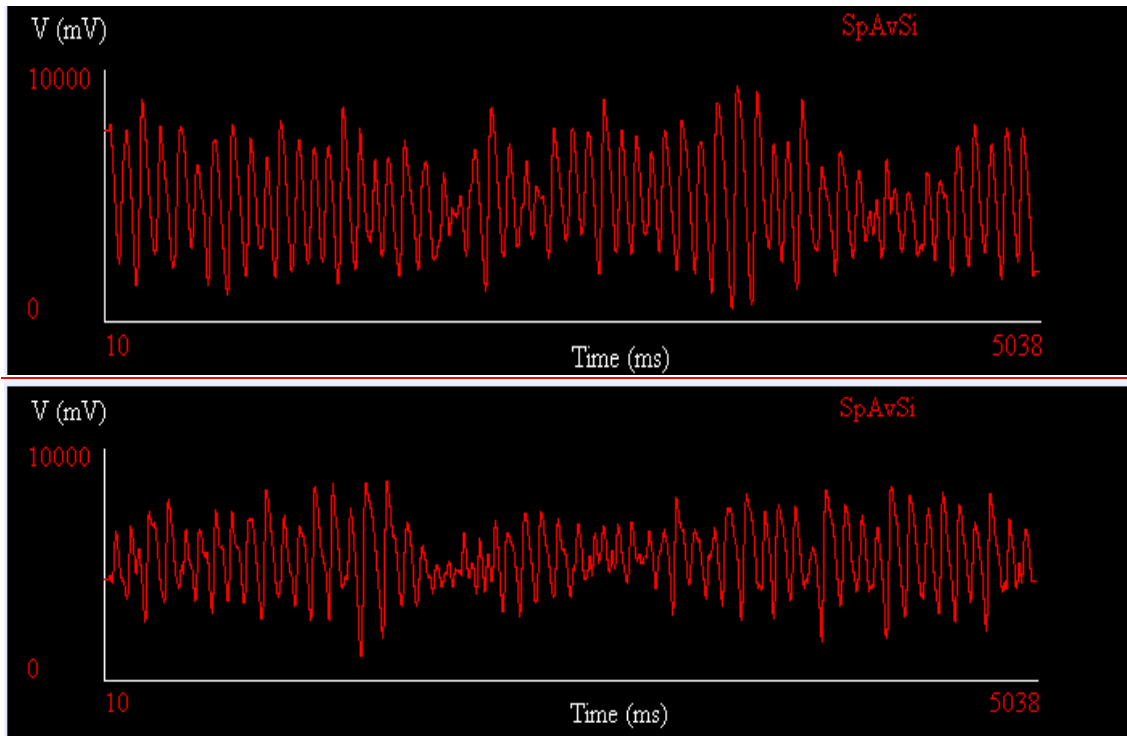


Figure 25. Two examples of time evolution taken from the analysis of two experiments: the irregular electrical waves are a sign that VF is rose. Time evolutions are of two different points in the endocardium. Each of them come from two different experiments. Potentials in normalized units.

4.1.2 The effects of hypocalcemia on the slope of the dynamic restitution curves and on alternans

The slope of the curve was the indicator suggested by Nolasco and Dahlen [1] to predict the onset of alternans but the experiments performed confirmed what was already pointed out in previous studies [2,3]: this is not a good criterion because it fails in several experimental situations. In tab. 2, the slopes of the dynamical restitution curves, calculated using the method mentioned at the beginning of this chapter, are shown. As clearly visible in the LC condition slopes are greater than with NT solution comparing endocardium NT with respect to endocardium LC and epicardium NT with respect to epicardium LC. As shown in fig. 26 and 29, the APD-DI restitution curve's slope in normal condition (inset in A) is smaller than the one in low calcium conditions (inset in B) and according to the Nolasco and Dahlen's criterion alternans should arise in low calcium condition too but, as shown in fig. 27 and 30, where bifurcations diagrams are presented, there is no onset of alternans in low calcium conditions. Only the differences between two APD at the same $CL \geq 4$ ms are considered alternans. Comparing the restitution curves in normal conditions and in low calcium condition there is the evidence of a prolongation of the APD at all CLs as displayed by the upward shift of the APD restitution curves and as reported by a previous study [4, 5].

	ENDO				NT						ENDO				LC			
	point 1	point 2	point 3	point 4	point 1	point 2	point 3	point 4			point 1	point 2	point 3	point 4	point 1	point 2	point 3	point 4
Slopes	0,083	0,041	0,019	0,079	0,053	0,05	0,05	0,045	Slopes	0,015	0,025	0,017	0,015	0,003	0,009	0,014	0,005	
	0,119	0,073	0,04	0,113	0,076	0,073	0,072	0,065		0,577	0,598	0,506	0,474	0,236	0,26	0,346	0,188	
	0,2	0,163	0,103	0,192	0,129	0,131	0,125	0,112		0,758	0,739	0,683	0,616	0,315	0,354	0,427	0,277	
	0,309	0,301	0,216	0,291	0,196	0,204	0,195	0,176		1,121	1,078	0,988	0,938	0,572	0,564	0,749	0,479	
	0,421	0,501	0,398	0,401	0,276	0,299	0,272	0,249		1,409	1,314	1,241	1,208	0,811	0,74	0,93	0,653	
	0,562	0,718	0,631	0,531	0,38	0,425	0,381	0,351		1,532	1,408	1,337	1,295	0,944	0,82	1,047	0,713	
	0,597	0,781	0,703	0,57	0,414	0,479	0,406	0,38		1,671	1,524	1,459	1,428	1,068	0,925	1,096	0,801	
	0,665	0,834	0,759	0,644	0,448	0,513	0,457	0,425		1,82	1,633	1,601	1,543	1,206	0,986	1,206	0,911	
	0,708	0,898	0,83	0,687	0,481	0,578	0,499	0,47		1,94	1,741	1,678	1,651	1,336	1,093	1,323	0,989	
	0,741	0,962	0,901	0,722	0,517	0,635	0,52	0,493		2,058	1,876	1,81	1,763	1,499	1,159	1,453	1,077	
	0,694	0,849	0,781	0,651	0,468	0,566	0,474	0,441		2,269	2,005	1,992	1,923	1,626	1,292	1,558	1,189	
	0,934	1,154	1,066	0,86	0,644	0,795	0,637	0,592		2,386	2,094	2,079	2,011	1,853	1,374	1,638	1,334	
	0,682	1,248	1,317	0,685	0,511	0,608	0,513	0,503		2,319	2,156	2,125	2,06	1,878	1,409	1,674	1,342	
	0,768	1,407	1,486	0,758	0,548	0,631	0,556	0,551		2,579	2,281	2,257	2,202	2,052	1,528	1,774	1,436	
	1,028	1,344	1,389	0,962	0,534	0,617	0,536	0,533		2,696	2,417	2,337	2,312	2,193	1,594	1,914	1,561	
	1,092	1,424	1,713	1,006	0,83	1,054	0,822	0,782		2,632	2,333	2,334	2,261	2,146	1,572	1,917	1,527	
	1,18	1,688	1,99	1,168	0,634	0,782	0,636	0,884		2,79	2,495	2,441	2,366	2,303	1,652	1,929	1,598	
	1,003	1,674	1,57	0,931	0,668	0,838	0,696	0,646		2,767	2,508	2,522	2,477	2,291	1,726	1,974	1,671	
	1,042	1,486	1,653	1,057	0,598	0,72	0,608	0,584		VF	VF	VF	VF	VF	VF	VF	VF	
	1,267	1,997	2,131	1,192	0,772	1,029	0,792	0,733										
MEAN	0,705	0,977	0,985	0,675	0,459	0,551	0,462	0,451	MEAN	1,852	1,679	1,634	1,586	1,352	1,059	1,276	0,986	
STAND.DEV.	0,349	0,567	0,651	0,334	0,219	0,289	0,224	0,233	STAND.DEV.	0,817	0,712	0,723	0,713	0,749	0,516	0,596	0,517	

	ENDO				NT						ENDO				LC			
	point 1	point 2	point 3	point 4	point 1	point 2	point 3	point 4			point 1	point 2	point 3	point 4	point 1	point 2	point 3	point 4
Slopes	0,051	0,052	0,055	0,065	0,053	0,055	0,042	0,024	Slopes	0,07	0,111	0,122	0,115	0,053	0,055	0,042	0,024	
	0,091	0,094	0,096	0,108	0,115	0,118	0,095	0,06		0,147	0,219	0,247	0,227	0,115	0,118	0,095	0,06	
	0,167	0,166	0,165	0,185	0,252	0,259	0,216	0,162		0,316	0,43	0,473	0,471	0,252	0,259	0,216	0,162	
	0,245	0,256	0,245	0,273	0,48	0,465	0,436	0,349		0,579	0,72	0,831	0,802	0,48	0,465	0,436	0,349	
	0,401	0,39	0,379	0,403	0,804	0,86	0,781	0,69		0,985	1,173	1,321	1,243	0,804	0,86	0,781	0,69	
	0,538	0,506	0,49	0,524	1,093	1,173	1,091	0,994		1,299	1,491	1,675	1,649	1,093	1,173	1,091	0,994	
	0,657	0,591	0,625	0,607	1,314	1,395	1,507	1,387		1,503	1,588	1,854	1,643	1,314	1,395	1,507	1,387	
	0,668	0,641	0,718	0,663	1,457	1,618	1,434	1,527		1,711	1,626	2,065	1,675	1,457	1,618	1,434	1,527	
	0,729	0,663	0,716	0,768	1,755	1,509	1,536	1,641		1,717	1,622	1,851	2,511	1,755	1,509	1,536	1,641	
	0,853	0,735	0,705	0,741	1,604	1,955	1,477	1,834		2,203	1,665	1,927	1,839	1,604	1,955	1,477	1,834	
	0,808	0,791	0,73	0,789	1,813	1,65	1,549	1,918		1,753	2,559	1,959	2,594	1,812	1,65	1,549	1,918	
	0,757	0,931	0,85	0,944	2,09	1,618	1,64	1,854		1,824	1,733	1,977	1,842	2,09	1,618	1,64	1,854	
	0,995	0,84	0,808	0,842	1,846	2,174	2,439	2,384		1,939	1,828	2,365	2,833	1,846	2,174	2,439	2,384	
	0,849	1,023	0,96	1,06	2,34	2,127	2,223	2,374		2,071	2,171	2,986	2,225	2,34	2,127	2,223	2,374	
	0,888	1,072	0,993	1,135	1,923	1,958	2,616	2,154		2,459	2,976	2,327	2,214	1,923	1,958	2,616	2,154	
	0,881	1,071	0,977	1,118	2,527	2,221	2,232	2,648		2,739	3,227	2,689	3,156	2,527	2,221	2,232	2,648	
	1,187	0,988	0,961	0,961	2,547	2,694	2,872	2,754		2,894	2,663	3,132	3,028	2,547	2,694	2,872	2,754	
	1,029	1,205	1,096	1,193	2,519	2,565	2,734	2,761		2,983	3,066	3,274	3,129	2,519	2,565	2,734	2,761	
	1,13	1,274	1,147	1,253	2,697	2,733	2,828	2,861		3,093	3,063	3,437	3,252	2,697	2,733	2,828	2,861	
	1,254	1,317	1,239	1,32	3,096	3,095	3,013	3,221		3,299	3,239	3,588	3,458	3,096	3,095	3,013	3,221	
	1,353	1,331	1,225	1,294	2,977	3,067	3,092	3,254		3,283	3,251	3,605	3,492	2,977	3,067	3,092	3,254	
	1,293	1,31	1,216	1,277	3,156	3,193	3,388	3,443		3,502	3,432	3,802	3,687	3,156	3,193	3,388	3,443	
	1,539	1,53	1,422	1,499	3,199	3,302	3,368	3,478		3,596	3,369	3,755	3,726	3,199	3,302	3,368	3,478	
	1,485	1,542	1,425	1,509	3,315	3,237	3,44	3,744		3,593	3,386	3,804	3,792	3,315	3,237	3,44	3,744	
	1,58	1,617	1,52	1,569	3,476	3,49	3,46	4,005		3,523	3,601	3,846	3,838	3,476	3,49	3,46	4,005	
	VF		VF	VF	VF	VF	VF	VF	VF	VF								
MEAN	0,857	0,877	0,831	0,884	1,938	1,941	1,98	2,061	MEAN	2,123	2,168	2,356	2,338	1,938	1,941	1,98	2,061	
STAND.DEV.	0,443	0,463	0,42	0,447	1,045	1,046	1,112	1,194	STAND.DEV.	1,126	1,095	1,164	1,155	1,045	1,046	1,112	1,194	

Tab. 2. The slopes of dynamic restitution curves. The slopes are calculated after fitting the experimental points with an exponential function. The value are displayed for each for the four chosen points in the endocardium end in the epicardium both in low calcium (LC) conditions and with normal Tyrode's solution (NT). The slopes became greater and greater for small DIs (as shown in fig. 26 and fig. 29). VF means that ventricular fibrillation has occurred. VF hasn't occurred in normal (NT) conditions in one experiment

Fig. 26 and 27 are referred to one experiment and to the endocardial side while fig. 29 and 30 are related to the same experiment but to the epicardial side. In fig. 28 is shown the 2 D spatial distribution obtained with the java code and referred to fig. 26 A: discordant alternans are displayed by tissue as clearly indicated by the presence of two regions (RED and BLUE) whit different phases, separated by the nodal line (WHITE) where there are no alternans as it is a transition zone between the two phases. To show the increment of APD under the low calcium condition graphs such as the one shown in fig. 31 are plotted for each experiments. These graphs compares all the restitution curves got in a same experiment from the endocardium in LC conditions and with NT solution. From such a graph is clearer the APD prolongation in low calcium conditions.

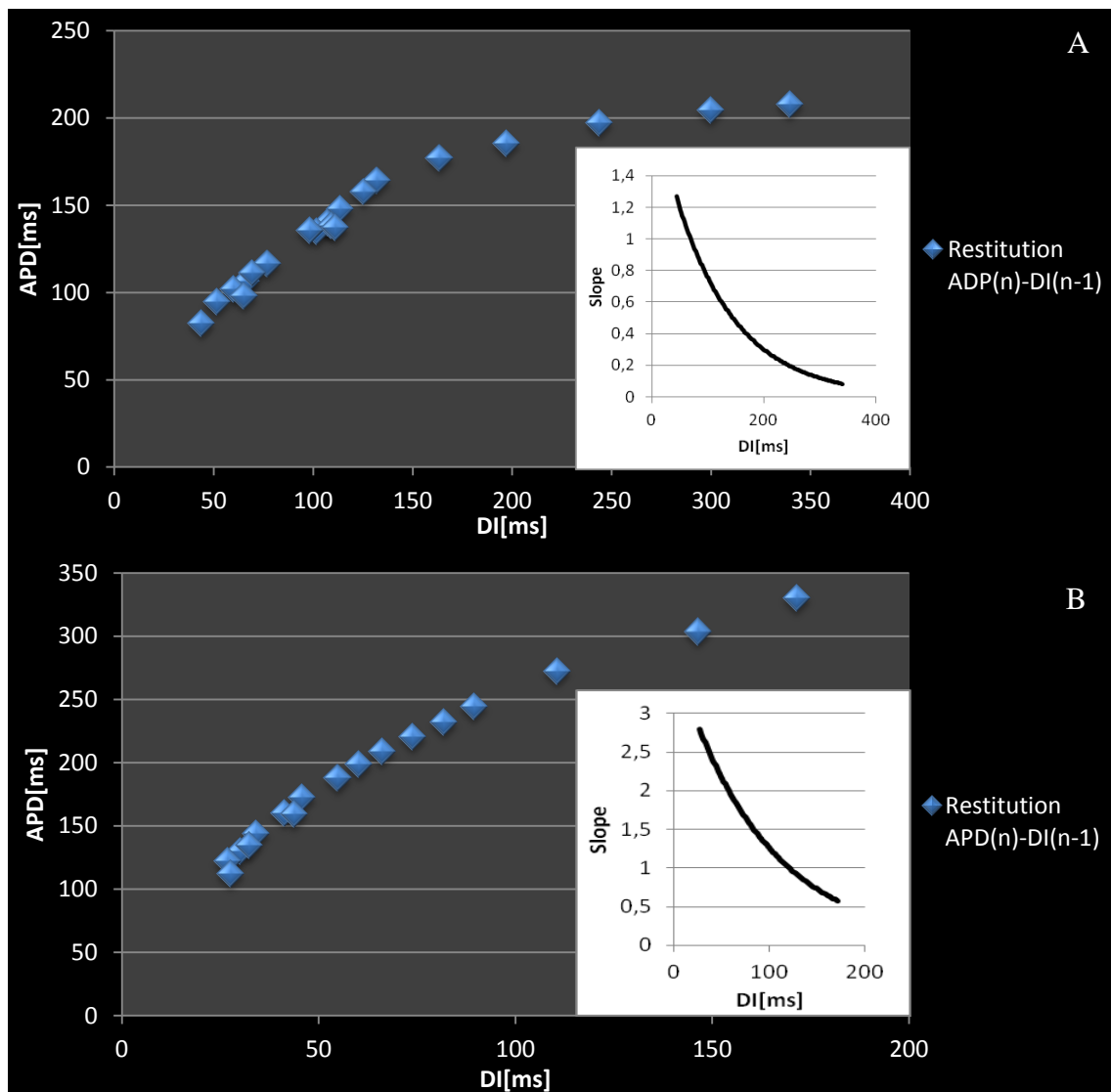


Figure 26. Dynamical restitution curves: A, physiological conditions (normal Tyrode, NT); B, low calcium condition (LC). The insets shows the curve's slopes: is clear that in B the slope is greater than in A. from these curves it also possible seeing that the APD values are greater in low calcium conditions (B) than in normal conditions (A).

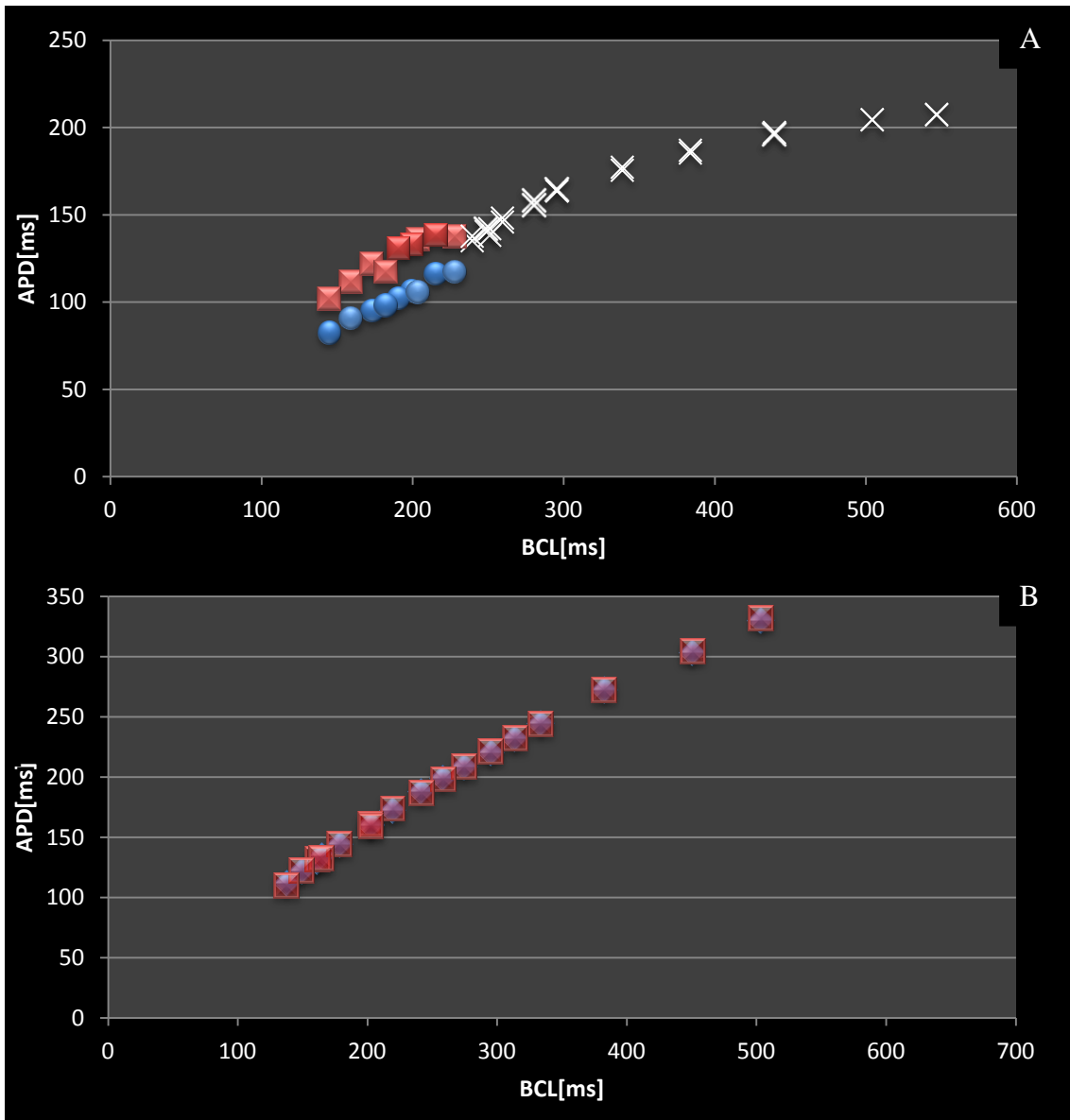


Figure 27. The bifurcation diagrams related to the restitution curves of fig.25. A, the bifurcation diagram in normal conditions: alternans, starting at a pacing rate of indicatively 250 ms, is evident; B, the bifurcation diagram in low calcium: no presence of alternans. This fact prove the failure of the Nolasco and Dahlen's criterion for predicting the onset of alternans.

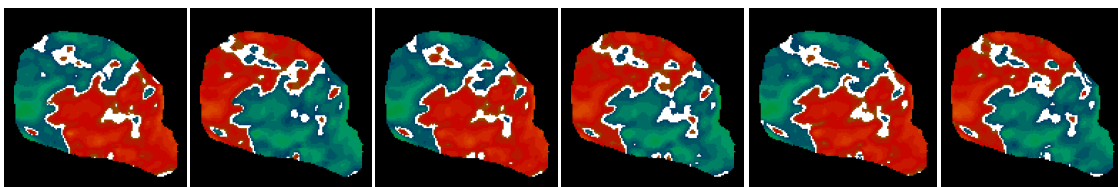


Figure 28. The spatial distribution of discordant alternans. This figure shows a sequence of six beats at a CL of 190 ms. This sequence shows the very same of fig. 27 A but from another point of view: while the restitution curve in fig. 26 A shows the 1-D dynamics, here it's shown the 2-D dynamics underlining one of the major feature of the paced tissue, the onset of discordant alternans which are indicated as a precursor and an indicator of ventricular fibrillation (VF).

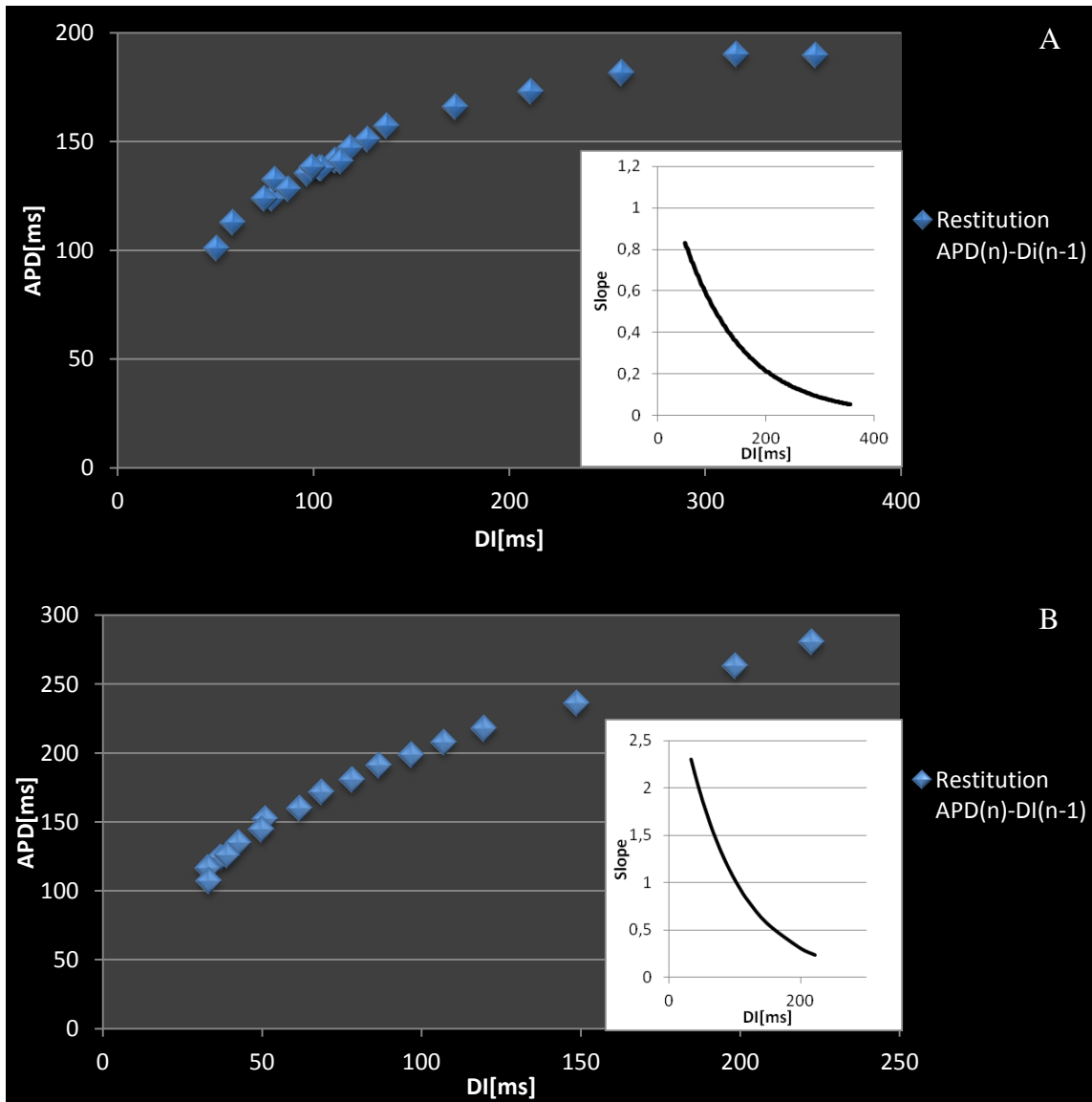


Figure 29. Dynamical restitution curves: A, physiological conditions (normal Tyrode, NT); B, low calcium condition (LC). The same considerations done in fig. 26 can be done for this figure keeping in mind that figure is referred to the epicardium.

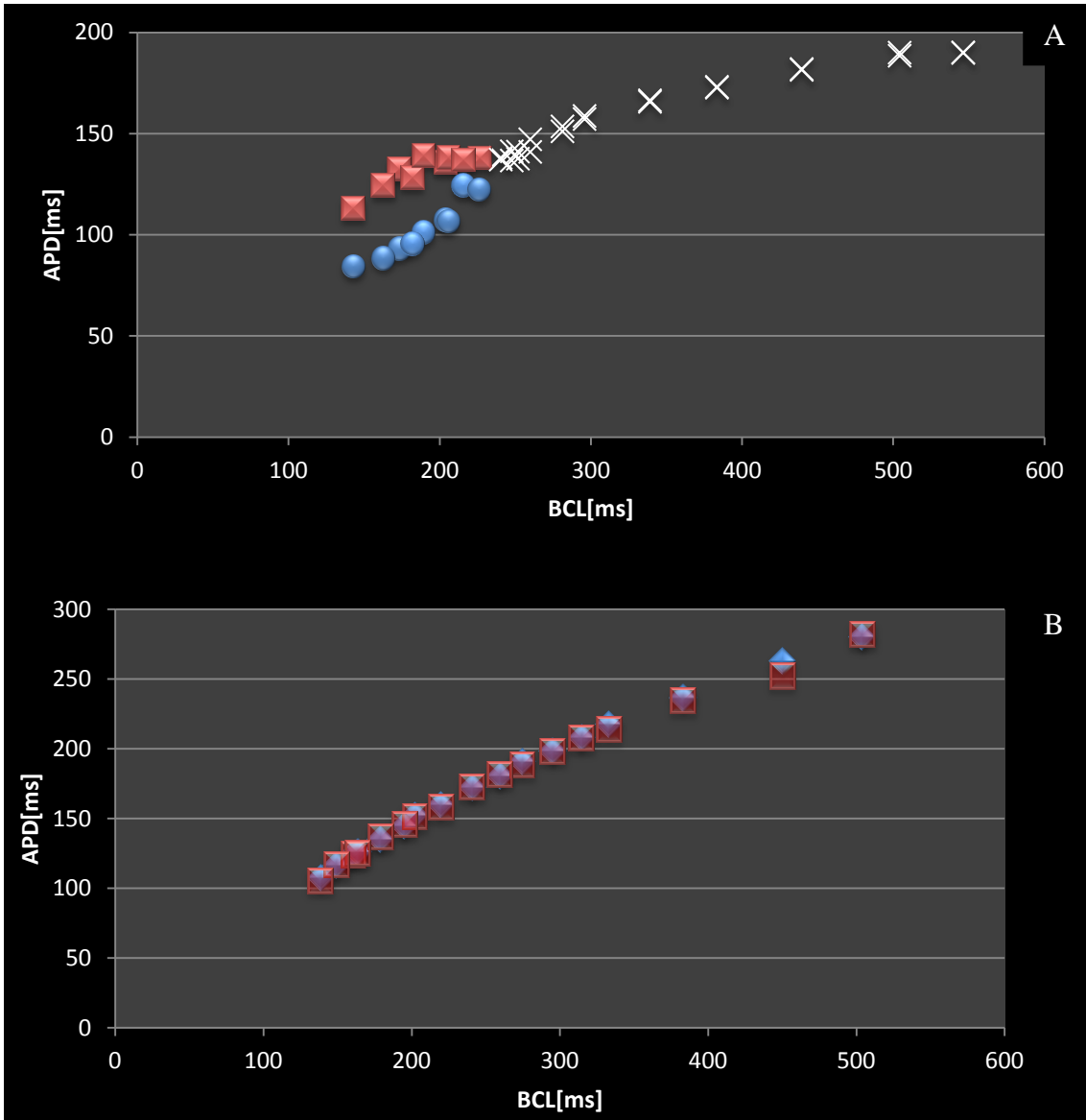


Figure 30. The bifurcation diagrams related to the restitution curves of fig. 29 (epicardium). A, bifurcation diagram in normal conditions; B, bifurcation diagram in low calcium. Splitting points at the same CL, persisting for enough beats, are considered alternans if the difference of the APDs is ≥ 4 ms.

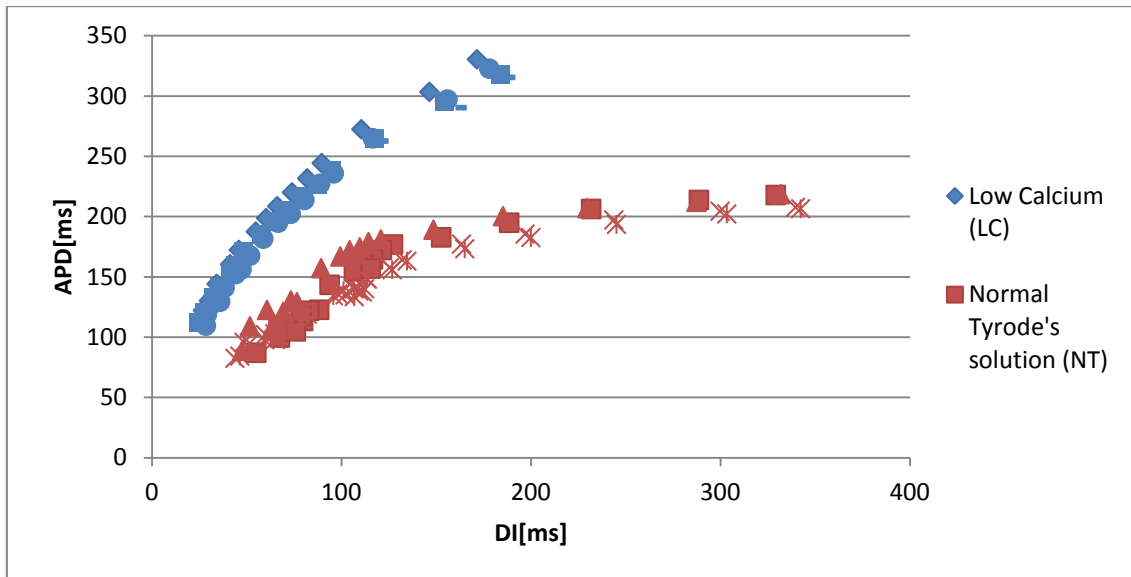


Figure 31. The effect of low calcium [0.0625 mM] (hypocalcemia) on APD amplitude. The comparison of the restitution curves shows that in low calcium conditions, the curves are upward shifted: this means that there is an increment of the APDs. This curve are obtain from 4 points on the endocardial surface both in normal and in low calcium conditions

In these experiment another scenario has been found: alternans appear and disappear forming a kind of eye in the bifurcation diagram, as it's shown in fig. 32. Also in this situation the criterion fails: in the point where alternans disappears the slope is greater than 1 and greater than in the point where alternans start. In such situations the amplitude of alternans is very small even if greater than 4 ms.

4.1.3 The effects of hypocalcemia On short-term memory

As it has been written in chapter 3 the short-term memory is connected to $[Ca^{2+}]_i$ [6]. In order to investigate this problem a dynamic-S1-S2 protocol was used and three experiments in low calcium condition were performed. In this study it has been thought to act on the $[Ca^{2+}]_i$ operating on the $[Ca^{2+}]_o$ that's why a low calcium concentration has been used. The intention was to block the calcium induced calcium release (CICR) stopping the inward calcium current. Doing this we obtained, first of all, the stop of all the muscular contraction and then, as shown in fig. 33, there is a downward shift of the S1-S2 restitution curves and there is no matching between the different restitution curves.

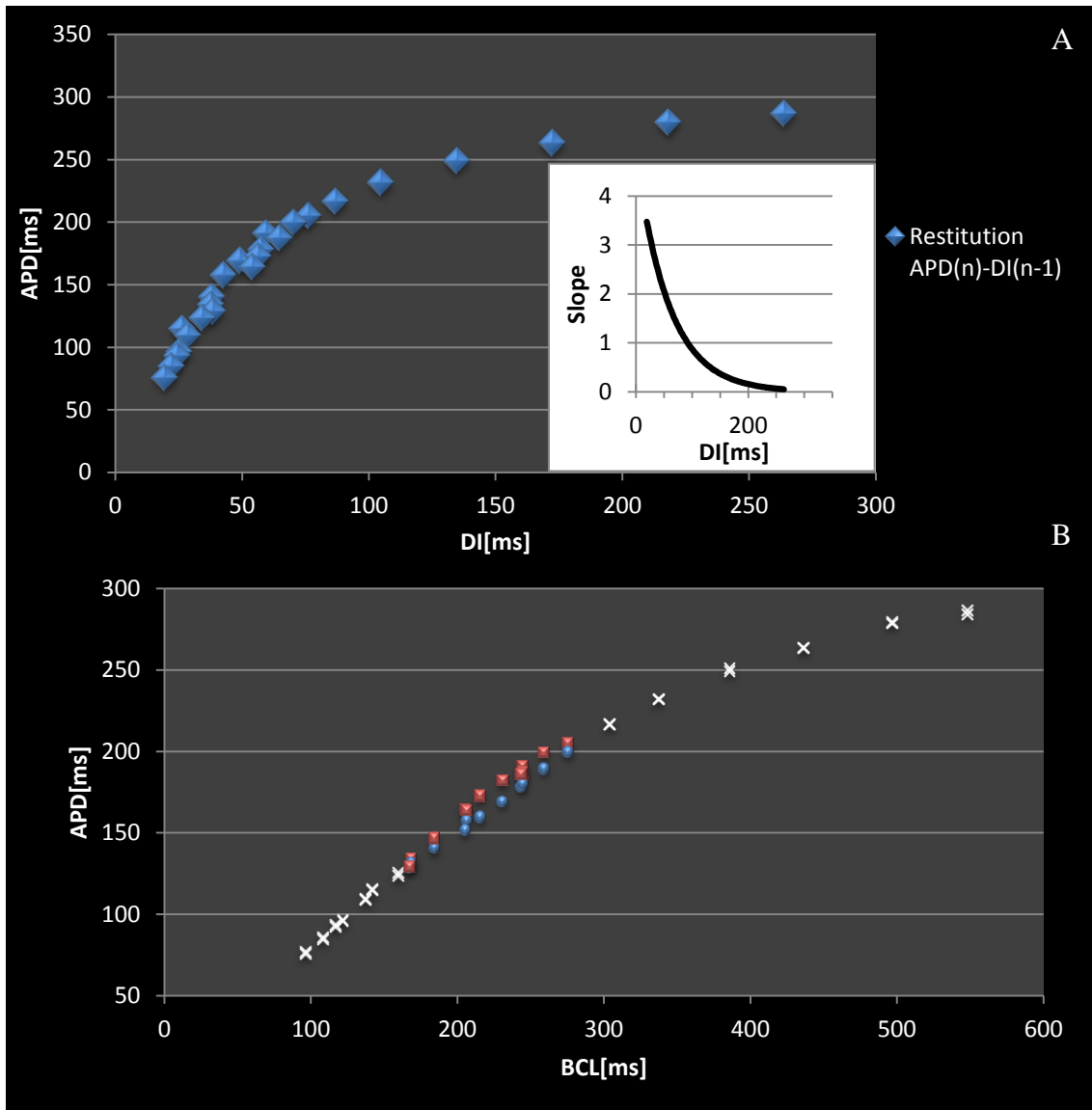


Figure 32. The dynamic restitution curve and the bifurcation diagram of the "eye scenario". These graphs are obtained in low calcium conditions from the epicardial side of a different experiment with respect to the other seen till now. For small DIs the slope the restitution curve became steeper and steeper thus favoring the onset of alternans, according to the Nolasco and Dahlen's criterion; actually, small alternans rise but, instead increasing in amplitude, the alternans disappears forming a sort of eye despite the slope is greater and greater.

4.1.4 The Tolkacheva's criterion

As said in point number 2, the Nolasco and Dahlen's criterion is not useful; moreover as previously underlined, the short-term memory is still present in low calcium condition. In such conditions the criterion developed by Tolkacheva [7] for one dimensional maps with memory was implemented. For the implementation the curves shown in fig. 33 were used. The new criterion was implemented in the intersection points [7, 8, 9] between the dynamic restitution curve and the S1-S2 restitution curves. It's important to remind that the intersection points are very accurate because of the particular protocol adopted: if the S1 stimulus is equal to the S2 stimulus, we are using no more the S1-S2 protocol but the Dynamical protocol. And so using the S1-S2 protocol, when $S1=S2$ we

are obtaining the same values than the Dynamical protocol. The values of the $|F'|$ got from different experiments and calculated as explained before, are shown in tab. 3. There is no evidence of alternans in the last three experiments and the criterion seems to confirm this result.

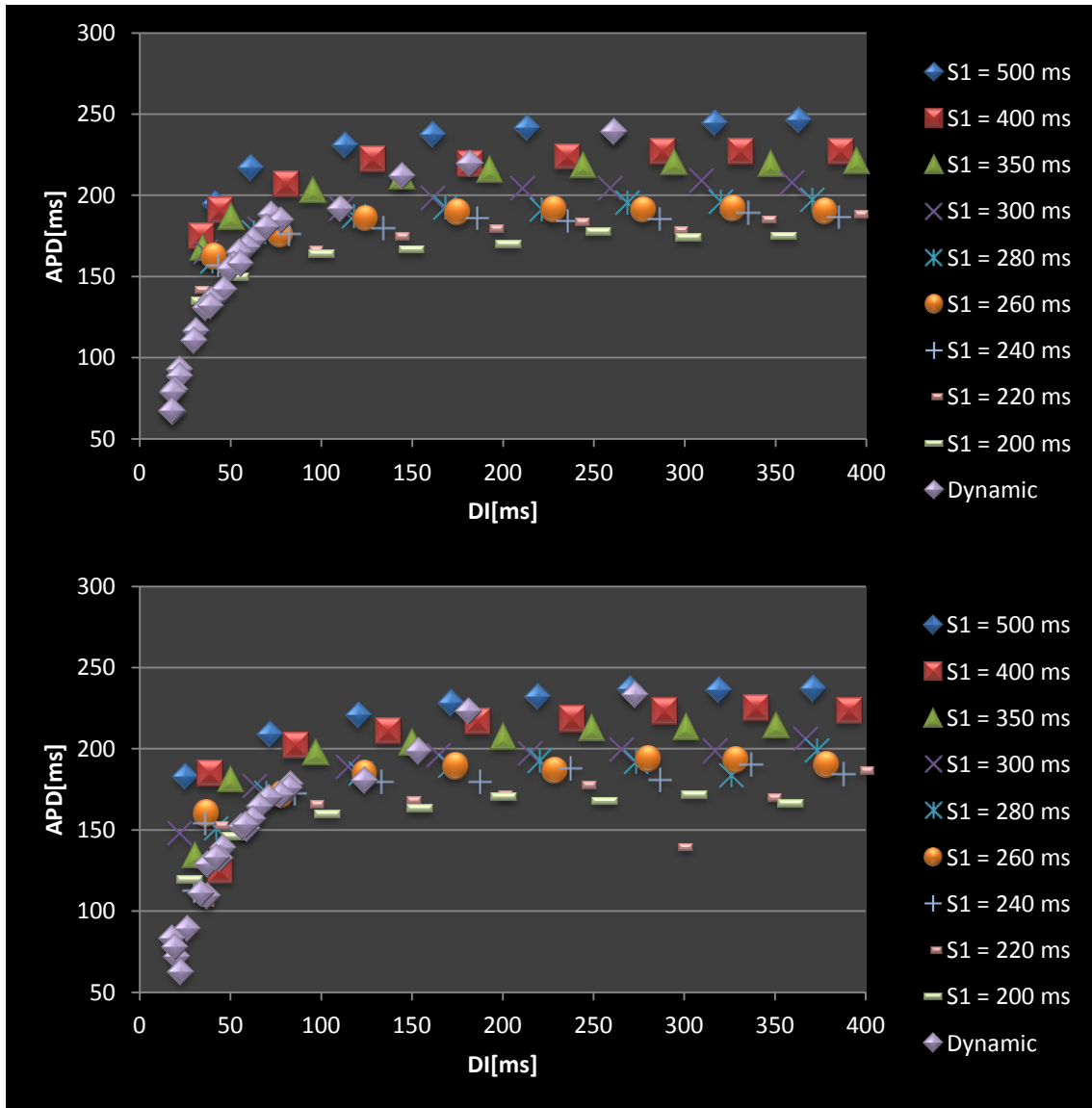


Figure 33. The restitution curves obtained with the Dynamical-S1-S2 protocol in two different experiments. For a better visualization the maximum of the DI's scale is 400 ms but actually the initial CL was 900 ms. Both in the up and in the bottom graph there is no a perfect matching of the curves. In according with some studies [7, 8] this mismatching is due to the short-term memory which is an intrinsic property of the pacing tissue. The experiments were performed in low calcium conditions and this seems having no effects on the memory, which still occurs. The same result can be observed in the other performed experiments with no difference between epicardium and endocardium.

$ \mathbf{F}' $ (exp. #3)	$ \mathbf{F}' $ (exp. #4)	$ \mathbf{F}' $ (exp. #5)
0,6	0,155	0,506
0,498	0,372	0,36
0,511	0,493	0,262
0,484	0,43	0,316
0,389	0,194	
0,336	0,297	
0,342	0,262	
0,103		
0,084		
0,618		

Tab. 2. The Chart shows the implementation of the Tolkacheva's criterion. In the columns, labeled $|\mathbf{F}'|$, there are the numerical values calculated directly with the formula. Each column represents one of the four points chosen on the epicardium or on the endocardium of the RV of an experiment. As it can be seen all the $|\mathbf{F}'|$ are smaller than 1 even though the slope of the dynamical restitution curve is greater than 1 (green values). The implementation of this criterion to all the other points lead to the same conclusions. The criterion seems working on low calcium condition.

4.2 Conclusions

This work, focusing on the study of effects of hypocalcemia, meaning a very low calcium concentration [0.0625 mM], on spatial alternans and ventricular fibrillation (VF), encompasses (covers) different aspects:

- the theoretical one, made up by the study of the underlying theory: medical, physical-mathematical and technical;
- the experimental one concerning in canine hearts explantation, the preparation of the tissue and of the Tyrode's solutions; also the arranging of the optical mapping set up and fixing hardware and software problems were dealt with no less than performing the experiments and collecting data following the protocols in the highest fidelity way;
- finally the computational one for the analysis and elaboration of data.

It's important underlining the complexity of this work in all its parts and the fact, common in all experimental works, that the initial target has been evolved during the ongoing because of the obtained results. All started off with the using of the dynamical protocol using a normal Tyrode's solution and a low calcium one. Two experiments were performed in such conditions. This means that two right ventricles (RV) have been used. Thanks to the optical mapping technique we have been able to recording the electrical activity both in the endocardium and in the epicardium, measuring the action potentials and in particular the APDs and the DIs in four points on both sides, in order

to plot the dynamical restitution curves and compare the normal conditions to the low calcium ones. The latter has produced a prolongations of the APDs and a steepness of the restitution curves which, according to the Nolasco and Dahalen's criterion [1], should mean the onset of alternans. Curiously there is no evidence of alternans in such a situation or we have the "eye" configuration: alternans appear and disappear. The question at the point is why alternans haven't risen even if the slope of the restitution curves are greater than 1. As suggested in some studies, the dependence on the previous DI is a rough approximation, and the APD restitution relation is not a solely function of the previous DI but it depends on memory, on conduction velocity (CV) and on other factor [8]; moreover experimentally the restitutions curves depend on the adopted protocol and these differences are determined by the short-term memory [7] which is related to the $[Ca^{2+}]_i$ [6]. It has been decided to performed other three experiments using a different pacing protocol, called Dynamical-S1-S2 protocol (which is a modified version of the perturbed downsweep protocol [7]), in order to study the effect of memory using a low calcium concentration. This fact, in our intensions, should block the CICR, (this was verisimilar because the muscular contractions stopped) and thus resetting the memory. What has been found is something unexpected: despite the low calcium concentration the memory effect is still present. The restitution curves haven't matched each other. This could mean that $[Ca^{2+}]_i$ is not involved in short term memory or is not the only factor; This results are in contradiction with a previous study where it was hypothesized that $[Ca^{2+}]_i$ plays an important role in short-term memory [6].

Finally we used another criterion to predict the onset of alternans: the Tolkacheva' criterion [7]. This criterion, based on a 1-D model with memory [3] where APD is a function of the previous DI and on the previous APD, considers the both the slope of the dynamical restitution curve and the slope of the S1-S2 restitution curves. The Tolkacheva's criterion, demonstrated till now only on rabbit [9], has given us good results in dogs using. Finally it's important spending few words upon the fact that we have been able to induce VF even in low calcium condition and with non alternans; this fact could mean that alternans is not the only mechanisms involved in the onset and maintenance of VF. The conclusions could be summed up in four points:

1. *In all cases studied (but one), presenting or not alternans, we are able to induce VF with fast pacing;*

2. *the slope of the curves in low calcium condition is even steeper than in normal condition and there is neither evidence of persistent alternans or alternans appear and disappear;*
3. *the memory effect doesn't depend on the extracellular calcium and hence on the sarcoplasmic calcium;*
4. *the criterion for alternans developed by Tolcacheva for a one dimensional map with memory is good working in low calcium conditions.*

4.3 Limitations and Future Works

In this work it has been mainly demonstrated that short-term memory doesn't depend on $[Ca^{2+}]_o$, and hence on $[Ca^{2+}]_i$; moreover it has been proofed the Tolcacheva's criterion in canine RV using the optical mapping technique; nevertheless, a great lack is present: it has been inferred from the results the non-dependence of the memory from $[Ca^{2+}]_i$ but there is no certainty that hypocalcemia, intended as extracellular low calcium concentration, abolished CICR even though all the studied RV displayed no muscular contraction. To better investigate the calcium transient an optical mapping analysis with a calcium sensitive dye could be performed. The memory effect was studied only on the base of the mismatching of the restitution curves and not even using the accommodation between two different CL [3, 6, 7] Another limit is in the fact that the experiments done to study the memory effect were performed only under condition of hypocalcemia thus missing a comparison with normal conditions. Even though the great support of the experimental data, the few experiments performed thus resulting in a lack of statistical analysis make impossible to be sure of the results which remains, for the moment, a mere speculation. Finally all the results are obtained from an excised canine RV: the heart is a complex organ and no one can say with precision if the mechanisms it has been seemed to identify will work in a whole human heart.

BIBLIOGRAPHY

- [1] J. B. Nolasco, and R. W. Dahlen. A graphic method for the study of alternation in cardiac action potentials. *J. Appl. Physiol.* 25, 191–196. 1968.
- [2] R. F. Gilmour, N. F. Otani, and M. A. Watanabe. Memory and complex dynamics in cardiac Purkinje fibers. *Am. J. Physiol.* 272: H1826_H1832, (1997)
- [3] N. F. Otani, and R. F. Gilmour. Memory models for electrical properties of local cardiac systems. *J. Theor. Biol.* 187: 409-436, 1997.
- [4] M. L. Riccio, F. Hua, D. J. Lomonte, K. R. Venator, S. Cerda-Gonzales, and R. F. Gilmour, Jr. Effects of Hypocacemia on electrical restitution and Ventricular Fibrillation. *31st Annual International Conference of the IEEE EMBS* Minneapolis, Minnesota, USA (2009).
- [5] E. Grandi, F. S. Pasqualini, C. Pes, C. Corsi, A. Zaza, S. Severi. Theoretical investigation of action potential duration dependance on extracellular Ca²⁺ in human cardimyocytes. *JMCC* . 46: 332-342 (2009).
- [6] H. Zang, T. Ueyama, J. Wang, RJ. Wu, and SF. Lin. Short-term and electrical restitution in the canine transmural ventricle. *Physiol. Meas.* 32:207-222 (2011).
- [7] E. G. Tolkacheva, D. G. Schaeffer, D. J. Gauthier, W. Krassowska. Condition for alternans and stability of the 1:1 response pattern in a “memory” model of paced cardiac dynamics. *Phys. Rev. E.* 67:031904 (2003).
- [8] Cherry, fenton. Suppression of alternans and conduction blocks despite steep APD restitution: electrotonic, memory, and conduction velocity restitution effects. *Am J Physiol Heart Circ Physiol* 286: H2332–H2341 (2004).
- [9] S. S. Kalb, H. M. Dobrovolny, E. G. Tolkacheva, S. F. Idriss, W. Krassowska, and D. Gauthier. The restitution portrait: A new method for investigating rate –dependent restitution. *J. Cardiovasc. Electrophysiol.* 15: 698-709 (2004)

Aknowledgments

First of all I wish to give thanks to my advisors, Prof. Stefano Severi, who gave me the possibility to do my thesis abroad and his support, leaving to me the possibility to choose the subject, and Prof. Flavio H. Fenton, who believed in me despite we never met before my arrival at Cornell University and introduced me to the experimental world. Thanks to my “American” friends and colleagues at Cornell: Prof. Gilmour, Fred, Niels, Jean, Danielle, Laura, Rupinder, Ayesa and Risheek; thanks to my Italian friends and special thanks to my “Italo-american” friends in NYC Tamhal and Valentina. Finally, I want to thank my parents, Giacomo and Patrizia, my brother, Matteo, and my whole family, and my girlfriend, Roberta: without their support and patience this work would never have been possible.